Available online at www.sciencedirect.com
SCIENCE DIRECT®
Journal of Computational Physics 202 (2005) 664–698
JOURNAL OF COMPUTATIONAL PHYSICS
www.elsevier.com/locate/jcp

A five equation reduced model for compressible two phase flow problems

Angelo Murrone [a,b,*], Hervé Guillard [b]

[a] CEA Cadarache, 13108 Saint-Paul-Lez-Durance, France
[b] INRIA, BP. 93, 06902 Sophia Antipolis Cedex, France

Received 21 January 2004; received in revised form 21 July 2004; accepted 29 July 2004
Available online 25 September 2004

Abstract

This paper studies an Eulerian diffuse interface model for the simulation of compressible multifluid and two-phase flow problems. We first show how to derive this model from a seven equation, two pressure, two velocity model of Baer–Nunziato type using an asymptotic analysis in the limit of zero relaxation time. We then study the mathematical properties of the system, the structure of the waves, the expression of the Riemann's invariants and the existence of a mathematical entropy. We also describe two different numerical approximation schemes for this system. The first one relies on a linearized Riemann solver while the second uses more heavily the mathematical structure of the system and relies on a linearization of the characteristic relations. Finally, we present some numerical experiments and comparisons with the results obtained by the two pressure, two velocity model as well as some test cases and comparisons with another five equation model recently proposed for interface computations between compressible fluids.

Keywords: Two phase flows; Compressible interface problems; Hyperbolic relaxation; Riemann solver; Non conservative products

1. Introduction

Modelling of two-phase flows is typically based on averaging procedures ([8,6]). In their most general form, these averaging techniques produce models characterized by two different velocities and

* Corresponding author. Present address: ONERA Chatillon, DEFA, 29 Avenue de la Division, Leclerc, BP 72, 92322 Chatillon, France. Tel.: +33146734320.
E-mail addresses: angelo.murrone@onera.fr (A. Murrone), herve.guillard@inria.fr (H. Guillard).

0021-9991/$ - see front matter
doi:10.1016/j.jcp.2004.07.019

pressures for each phase supplemented by one or several topological equations. Thus, in one dimension and for non-isentropic flows, a two-phase model of this type consists of at least seven equations (two mass conservation equations, two momentum equations, two energy (or pressure) equations plus one topological equation). These type of models have been known for a long time [3,15,19], but have been seldom used due to their complexity. However, some recent works [16] have shown that they possess several advantages over the more classical 6 equation system: these models are unconditionally hyperbolic, they are able to treat multiphase mixtures as well as interface problems between pure fluids and they allow the treatment of fluids characterized by very different thermodynamics because each fluid uses its own equation of state. However these models are numerically complex to solve because of the large number of waves they contain and of the sensibility of the results with respect to the relaxation procedures. These facts motivate the research of cheaper models. In particular, there is nowadays a growing interest in the application of two phase flows models to the simulation of interfaces between two immiscible compressible fluid by Eulerian diffuse interface methods. In these methods, numerical diffusion is responsible for the creation of an artificial transition region between the pure fluids. A mixture model has thus to be used to compute the flow inside this region. A sound physical modelling of this mixture region is to consider it as a true multiphase region. However, at the present time, the adequate level of complexity of the models used in this region is still a matter of debate. In [16], a seven equation complex model of Baer–Nunziato type was used. On the opposite, a very simple four equation multicomponent Euler system as in [1] can also be employed and as usual, a delicate balance between the complexity of the model and its performance have to be found. This work, thus explores the possibility to use an average way between these two extremes by constructing a five equation model suitable for some two-phase problems. In this respect, this contribution is similar in spirit to the works of Massoni et al. [12] and Allaire et al. [2] who recently proposed five equation models for the simulation of interfaces between compressible interfaces. However, in contrast with these previous works, we derive the five equation model by an asymptotic analysis of the seven equation model in the limit of zero relaxation times instead of using a priori closures. The procedure we use in this paper is therefore similar to the one proposed for detonation studies in [9]. The rationale for this approach is that we believe that due to a lack of computer resources, many interface computations are actually done with a poor spatial resolution with the results that the artificial diffusion zones can be quite large. In these situations, it may be safer to use a model that carries a maximum of physical informations.

The summary of this work is as follows. In Section 2, we give a brief description of the seven equation model. Then we perform an asymptotic analysis of this model for zero relaxation times and obtain a limit system characterized in one dimension by five partial differential equations. In Section 3, we study the mathematical properties of this reduced model; in particular we show that it is an unconditional hyperbolic system whatever the state laws of the pure fluids are. We study its mathematical structure and prove that the system contains fields which are either genuinely non linear or linearly degenerate and finally, we give the expression of the Riemann's invariants. Then in Section 4, we study two numerical procedures to solve this system. These numerical techniques do not require any hypothesis on the equation of state of each fluid. The first one of VFRoe-ncv type (see [4]) is based on the solution of a linearized Riemann's problem written in "entropic" variables. The second numerical scheme uses more heavily the mathematical structure of the reduced system and is an extension of the acoustic solver described for instance in [20] for the Euler system of gas dynamics. With respect to the different numerical test, the acoustic solver seems to be more robust than the VFRoe-ncv one when computing low Mach number two-phase flows. Finally in Section 5, the model have been applied to several difficult physical problems. In each case, the method provides reliable results, is able to compute strong shock waves, and to deal with interface problems occurring in compressible multifluid flows.

2. Derivation of the model

2.1. The seven equation model

The starting point of this study is the seven equation model presented in [16] which is a slight variation of the Baer–Nunziato 1986 model [3]. In term of conservative variables ${}^t(\alpha_k\rho_k,\alpha_k\rho_k\boldsymbol{u}_k,\alpha_k\rho_k e_k,\alpha_2)$, this model can be written:

$$\frac{\partial \alpha_1\rho_1}{\partial t} + \operatorname{div}(\alpha_1\rho_1\boldsymbol{u}_1) = 0, \tag{1.1}$$

$$\frac{\partial \alpha_1\rho_1\boldsymbol{u}_1}{\partial t} + \operatorname{div}(\alpha_1\rho_1\boldsymbol{u}_1\otimes\boldsymbol{u}_1) + \nabla\alpha_1 p_1 = p_{\mathrm{I}}\nabla\alpha_1 + \lambda(\boldsymbol{u}_2-\boldsymbol{u}_1), \tag{1.2}$$

$$\frac{\partial \alpha_1\rho_1 e_1}{\partial t} + \operatorname{div}(\alpha_1\rho_1 e_1 + \alpha_1 p_1)\boldsymbol{u}_1 = p_{\mathrm{I}}\frac{\partial\alpha_2}{\partial t} + \lambda\boldsymbol{u}_{\mathrm{I}}\cdot(\boldsymbol{u}_2-\boldsymbol{u}_1), \tag{1.3}$$

$$\frac{\partial \alpha_2\rho_2}{\partial t} + \operatorname{div}(\alpha_2\rho_2\boldsymbol{u}_2) = 0, \tag{1.4}$$

$$\frac{\partial \alpha_2\rho_2\boldsymbol{u}_2}{\partial t} + \operatorname{div}(\alpha_2\rho_2\boldsymbol{u}_2\otimes\boldsymbol{u}_2) + \nabla\alpha_2 p_2 = p_{\mathrm{I}}\nabla\alpha_2 - \lambda(\boldsymbol{u}_2-\boldsymbol{u}_1), \tag{1.5}$$

$$\frac{\partial \alpha_2\rho_2 e_2}{\partial t} + \operatorname{div}(\alpha_2\rho_2 e_2 + \alpha_2 p_2)\boldsymbol{u}_2 = -p_{\mathrm{I}}\frac{\partial\alpha_2}{\partial t} - \lambda\boldsymbol{u}_{\mathrm{I}}\cdot(\boldsymbol{u}_2-\boldsymbol{u}_1), \tag{1.6}$$

$$\frac{\partial \alpha_2}{\partial t} + \boldsymbol{u}_{\mathrm{I}}\cdot\nabla\alpha_2 = \mu(p_2-p_1). \tag{1.7}$$

The notations are classical. α_k are the volume fractions of each phase ($\alpha_1 + \alpha_2 = 1$), ρ_k the phase densities, $\boldsymbol{u}_k$ the vector velocities, p_k the pressures and $e_k = \varepsilon_k + \boldsymbol{u}_k^2/2$ the specific total energies, with ε_k the specific internal energies. On the other hand, p_{I} and $\boldsymbol{u}_{\mathrm{I}}$ stand for the interfacial pressure and velocity. In the Baer–Nunziato 1986 model [3], these variables are chosen as $p_{\mathrm{I}} = p_2$ and $\boldsymbol{u}_{\mathrm{I}} = \boldsymbol{u}_1$. But other choices are possible and for instance in [16], Saurel and Abgrall take the following interfacial values:

$$\boldsymbol{u}_{\mathrm{I}} = \sum_{k=1}^{2}\alpha_k\rho_k\boldsymbol{u}_k \Bigg/ \sum_{k=1}^{2}\alpha_k\rho_k \quad \text{and} \quad p_{\mathrm{I}} = \sum_{k=1}^{2}\alpha_k p_k. \tag{2}$$

We note that the choice of interfacial velocity and pressure can have a deep impact on the structure of the waves present in this model and on the fulfilment of entropy inequalities (see [5]). However, in this paper as we will assume that the phase pressures and velocities relax to a common value, these choices are not important and will not affect the derivation of the reduced model. Actually, the model (1) contains relaxation parameters λ and $\mu > 0$ that determine the rates at which the velocities and pressures of the two-phases reach equilibrium. The rationale for the introduction of such terms is discussed for instance in [16]. Here we are interested in situations where the relaxation times are small compared with the others characteristic times of the flow. Thus we set $\lambda = \lambda'/\varepsilon$ and $\mu = \mu'/\varepsilon$ where λ' and μ' are $\mathcal{O}(1)$ and we will analyse the case $\varepsilon \to 0$. This analysis can be performed directly on the system (1) with the conservative variables ${}^t(\alpha_k\rho_k,\alpha_k\rho_k\boldsymbol{u}_k,\alpha_k\rho_k e_k,\alpha_2)$, however it is more convenient to work with the set of variables ${}^t(s_k,\boldsymbol{u}_k,p_k,\alpha_2)$ where s_k are the phase entropies and to use the quasi-linear form of the equations. This is the purpose of the following section.

2.2. Quasi-linear "entropic" form of the model

In the sequel, the material derivative of a quantity ϕ with respect to the velocities $\boldsymbol{u}_k$ of each phase k as well as the interfacial velocity $\boldsymbol{u}_\mathrm{I}$ will be denoted by

$$\frac{\mathrm{D}_k\phi}{\mathrm{D}t} = \frac{\partial\phi}{\partial t} + \boldsymbol{u}_k \cdot \nabla\phi \quad \text{for } k = 1, 2 \text{ and } k = \mathrm{I}. \tag{3}$$

Using this notation, the momentum Eqs. (1.2)–(1.5) and the mass conservation Eqs. (1.1)–(1.4), it is easily seen that the velocities $\boldsymbol{u}_k$ obey the following equations:

$$\alpha_1\rho_1\frac{\mathrm{D}_1\boldsymbol{u}_1}{\mathrm{D}t} + \nabla\alpha_1 p_1 = p_\mathrm{I}\nabla\alpha_1 + \lambda(\boldsymbol{u}_2 - \boldsymbol{u}_1), \tag{4.1}$$

$$\alpha_2\rho_2\frac{\mathrm{D}_2\boldsymbol{u}_2}{\mathrm{D}t} + \nabla\alpha_2 p_2 = p_\mathrm{I}\nabla\alpha_2 - \lambda(\boldsymbol{u}_2 - \boldsymbol{u}_1) \tag{4.2}$$

from which we deduce the equations for the kinetic energies $\boldsymbol{u}_k^2/2$ of each phase:

$$\alpha_1\rho_1\frac{\mathrm{D}_1\boldsymbol{u}_1^2/2}{\mathrm{D}t} + \boldsymbol{u}_1 \cdot \nabla\alpha_1 p_1 = p_1\boldsymbol{u}_1 \cdot \nabla\alpha_1 + \lambda\boldsymbol{u}_1 \cdot (\boldsymbol{u}_2 - \boldsymbol{u}_1), \tag{5.1}$$

$$\alpha_2\rho_2\frac{\mathrm{D}_2\boldsymbol{u}_2^2/2}{\mathrm{D}t} + \boldsymbol{u}_2 \cdot \nabla\alpha_2 p_2 = p_1\boldsymbol{u}_2 \cdot \nabla\alpha_2 - \lambda\boldsymbol{u}_2 \cdot (\boldsymbol{u}_2 - \boldsymbol{u}_1). \tag{5.2}$$

From (5.1) and (5.2), using $e_k = \varepsilon_k + \boldsymbol{u}_k^2/2$ and the total energy Eqs. (1.3)–(1.6), we get the equations for the specific internal energies ε_k:

$$\alpha_1\rho_1\frac{\mathrm{D}_1\varepsilon_1}{\mathrm{D}t} + \alpha_1 p_1 \mathrm{div}\boldsymbol{u}_1 = p_\mathrm{I}(\boldsymbol{u}_\mathrm{I} - \boldsymbol{u}_1) \cdot \nabla\alpha_1 + \mu p_\mathrm{I}(p_2 - p_1) + \lambda(\boldsymbol{u}_\mathrm{I} - \boldsymbol{u}_1) \cdot (\boldsymbol{u}_2 - \boldsymbol{u}_1), \tag{6.1}$$

$$\alpha_2\rho_2\frac{\mathrm{D}_2\varepsilon_2}{\mathrm{D}t} + \alpha_2 p_2 \mathrm{div}\boldsymbol{u}_2 = p_\mathrm{I}(\boldsymbol{u}_\mathrm{I} - \boldsymbol{u}_2) \cdot \nabla\alpha_2 - \mu p_\mathrm{I}(p_2 - p_1) - \lambda(\boldsymbol{u}_\mathrm{I} - \boldsymbol{u}_2) \cdot (\boldsymbol{u}_2 - \boldsymbol{u}_1). \tag{6.2}$$

Next, using the volume fraction Eq. (1.7), it is easily seen that we can rewrite the mass conservation Eqs. (1.1)–(1.4) in term of phasic densities ρ_k under the form:

$$\alpha_1\frac{\mathrm{D}_1\rho_1}{\mathrm{D}t} + \alpha_1\rho_1 \mathrm{div}\boldsymbol{u}_1 = \rho_1(\boldsymbol{u}_\mathrm{I} - \boldsymbol{u}_1) \cdot \nabla\alpha_1 + \mu\rho_1(p_2 - p_1), \tag{7.1}$$

$$\alpha_2\frac{\mathrm{D}_2\rho_2}{\mathrm{D}t} + \alpha_2\rho_2 \mathrm{div}\boldsymbol{u}_2 = \rho_2(\boldsymbol{u}_\mathrm{I} - \boldsymbol{u}_2) \cdot \nabla\alpha_2 - \mu\rho_2(p_2 - p_1). \tag{7.2}$$

To obtain the equations for the phase entropies s_k, we use the Gibb's relation for each phase k

$$\mathrm{d}\varepsilon_k = T_k \mathrm{d}s_k + \frac{p_k}{\rho_k^2}\mathrm{d}\rho_k \quad \text{for } k = 1, 2, \tag{8}$$

where T_k is the temperature of phase k. Taking the material derivative of the Gibb's relation (8) and multiplying by $\alpha_k\rho_k$ we get

$$\alpha_k\rho_k T_k\frac{\mathrm{D}_k s_k}{\mathrm{D}t} = \alpha_k\rho_k\frac{\mathrm{D}_k\varepsilon_k}{\mathrm{D}t} - \frac{\alpha_k p_k}{\rho_k}\frac{\mathrm{D}_k\rho_k}{\mathrm{D}t} \quad \text{for } k = 1, 2 \tag{9}$$

from which we deduce with (6.1)–(7.2) the equations for the phase entropies s_k:

$$\alpha_1\rho_1 T_1\frac{\mathrm{D}_1 s_1}{\mathrm{D}t} = (p_\mathrm{I} - p_1)(\boldsymbol{u}_\mathrm{I} - \boldsymbol{u}_1) \cdot \nabla\alpha_1 + \mu(p_\mathrm{I} - p_1)(p_2 - p_1) + \lambda(\boldsymbol{u}_\mathrm{I} - \boldsymbol{u}_1) \cdot (\boldsymbol{u}_2 - \boldsymbol{u}_1), \tag{10.1}$$

$$\alpha_2\rho_2 T_2 \frac{\mathrm{D}_2 s_2}{\mathrm{D}t} = (p_\mathrm{I} - p_2)(\boldsymbol{u}_\mathrm{I} - \boldsymbol{u}_2)\cdot\nabla\alpha_2 - \mu(p_\mathrm{I} - p_2)(p_2 - p_1) - \lambda(\boldsymbol{u}_\mathrm{I} - \boldsymbol{u}_2)\cdot(\boldsymbol{u}_2 - \boldsymbol{u}_1). \tag{10.2}$$

Finally, to get the equations for the pressures p_k of each phase, we write that $p_k = p_k(\rho_k, s_k)$ and obtain the following expression for the differential $\mathrm{d}p_k$:

$$\mathrm{d}p_k = \left(\frac{\partial p_k}{\partial \rho_k}\right)_{s_k} \mathrm{d}\rho_k + \left(\frac{\partial p_k}{\partial s_k}\right)_{\rho_k} \mathrm{d}s_k \quad \text{for } k = 1, 2. \tag{11}$$

Now introducing the coefficients $\chi_k = (\partial\varepsilon_k/\partial\rho_k)_{p_k}$ and $\kappa_k = (\partial\varepsilon_k/\partial p_\mathrm{k})_{\rho_k}$, we write the differential of the specific internal energies ε_k under the following form:

$$\mathrm{d}\varepsilon_k = \chi_k \mathrm{d}\rho_k + \kappa_k \mathrm{d}p_k \quad \text{for } k = 1, 2. \tag{12}$$

Writing the equality of (8) and (12), solving for the differential of the pressure and comparing with (11) we get the well-known relations

$$a_k^2 = \left(\frac{\partial p_k}{\partial \rho_k}\right)_{s_k} = \frac{1}{\kappa_k}\left(\frac{p_k}{\rho_k^2} - \chi_k\right) \quad \text{and} \quad \left(\frac{\partial p_k}{\partial s_k}\right)_{\rho_k} = \frac{T_k}{\kappa_k} \quad \text{for } k = 1, 2, \tag{13}$$

where a_k denotes the sound speed of each phase. Now from (11)–(13) and after multiplication by the volume fraction α_k, we obtain the relation

$$\alpha_k \frac{\mathrm{D}_k p_k}{\mathrm{D}t} = \frac{\alpha_k}{\kappa_k}\left(\frac{p_k}{\rho_k^2} - \chi_k\right)\frac{\mathrm{D}_k \rho_k}{\mathrm{D}t} + \frac{\alpha_k T_k}{\kappa_k}\frac{\mathrm{D}_k s_k}{\mathrm{D}t} \quad \text{for } k = 1, 2 \tag{14}$$

from which we deduce with (7.1), (7.2), (10.1) and (10.2) the equations for the pressures p_k of each phase:

$$\begin{aligned}\alpha_1 \frac{\mathrm{D}_1 p_1}{\mathrm{D}t} + \alpha_1\rho_1 a_1^2 \mathrm{div}\boldsymbol{u}_1 = {} & \frac{\rho_1}{\kappa_1}\left(\frac{p_\mathrm{I}}{\rho_1^2} - \chi_1\right)(\boldsymbol{u}_\mathrm{I} - \boldsymbol{u}_1)\cdot\nabla\alpha_1 + \mu\frac{\rho_1}{\kappa_1}\left(\frac{p_\mathrm{I}}{\rho_1^2} - \chi_1\right)(p_2 - p_1) \\ & + \frac{\lambda}{\kappa_1\rho_1}(\boldsymbol{u}_\mathrm{I} - \boldsymbol{u}_1)\cdot(\boldsymbol{u}_2 - \boldsymbol{u}_1),\end{aligned} \tag{15.1}$$

$$\begin{aligned}\alpha_2 \frac{\mathrm{D}_2 p_2}{\mathrm{D}t} + \alpha_2\rho_2 a_2^2 \mathrm{div}\boldsymbol{u}_2 = {} & \frac{\rho_2}{\kappa_2}\left(\frac{p_\mathrm{I}}{\rho_2^2} - \chi_2\right)(\boldsymbol{u}_\mathrm{I} - \boldsymbol{u}_2)\cdot\nabla\alpha_2 - \mu\frac{\rho_2}{\kappa_2}\left(\frac{p_\mathrm{I}}{\rho_2^2} - \chi_2\right)(p_2 - p_1) \\ & - \frac{\lambda}{\kappa_2\rho_2}(\boldsymbol{u}_\mathrm{I} - \boldsymbol{u}_2)\cdot(\boldsymbol{u}_2 - \boldsymbol{u}_1).\end{aligned} \tag{15.2}$$

Finally introducing the notation $a_{k\mathrm{I}}^2 = (p_\mathrm{I}/\rho_k^2 - \chi_k)/\kappa_k$, where $a_{k\mathrm{I}}$ stands for the sound speed of the phase k at the interface, we can rewrite Eqs. (15.1) and (15.2) under the form:

$$\alpha_1 \frac{\mathrm{D}_1 p_1}{\mathrm{D}t} + \alpha_1\rho_1 a_1^2 \mathrm{div}\boldsymbol{u}_1 = \rho_1 a_{1\mathrm{I}}^2\,(\boldsymbol{u}_\mathrm{I} - \boldsymbol{u}_1)\cdot\nabla\alpha_1 + \mu\rho_1 a_{1\mathrm{I}}^2\,(p_2 - p_1) + \frac{\lambda}{\kappa_1\rho_1}(\boldsymbol{u}_\mathrm{I} - \boldsymbol{u}_1)\cdot(\boldsymbol{u}_2 - \boldsymbol{u}_1), \tag{16.1}$$

$$\alpha_2 \frac{\mathrm{D}_2 p_2}{\mathrm{D}t} + \alpha_2\rho_2 a_2^2 \mathrm{div}\boldsymbol{u}_2 = \rho_2 a_{2\mathrm{I}}^2\,(\boldsymbol{u}_\mathrm{I} - \boldsymbol{u}_2)\cdot\nabla\alpha_2 - \mu\rho_2 a_{2\mathrm{I}}^2\,(p_2 - p_1) - \frac{\lambda}{\kappa_2\rho_2}(\boldsymbol{u}_\mathrm{I} - \boldsymbol{u}_2)\cdot(\boldsymbol{u}_2 - \boldsymbol{u}_1). \tag{16.2}$$

Let us summarize the results of this section. In term of "entropic" variables ${}^t(s_k, \boldsymbol{u}_k, p_k, \alpha_2)$, the seven equation model (1) can be written under the quasi-linear form:

$$\alpha_1\rho_1 T_1 \frac{\mathrm{D}_1 s_1}{\mathrm{D}t} = (p_\mathrm{I} - p_1)(\boldsymbol{u}_\mathrm{I} - \boldsymbol{u}_1)\cdot\nabla\alpha_1 + \mu(p_\mathrm{I} - p_1)(p_2 - p_1) + \lambda(\boldsymbol{u}_\mathrm{I} - \boldsymbol{u}_1)\cdot(\boldsymbol{u}_2 - \boldsymbol{u}_1), \tag{17.1}$$

$$\alpha_2\rho_2 T_2 \frac{\mathrm{D}_2 s_2}{\mathrm{D}t} = (p_\mathrm{I} - p_2)(\boldsymbol{u}_\mathrm{I} - \boldsymbol{u}_2)\cdot\nabla\alpha_2 - \mu(p_\mathrm{I} - p_2)(p_2 - p_1) - \lambda(\boldsymbol{u}_\mathrm{I} - \boldsymbol{u}_2)\cdot(\boldsymbol{u}_2 - \boldsymbol{u}_1), \tag{17.2}$$

$$\alpha_1\rho_1\frac{\mathrm{D}_1\boldsymbol{u}_1}{\mathrm{D}t}+\nabla\alpha_1 p_1 = p_{\mathrm{I}}\nabla\alpha_1+\lambda(\boldsymbol{u}_2-\boldsymbol{u}_1), \tag{17.3}$$

$$\alpha_2\rho_2\frac{\mathrm{D}_2\boldsymbol{u}_2}{\mathrm{D}t}+\nabla\alpha_2 p_2 = p_{\mathrm{I}}\nabla\alpha_2-\lambda(\boldsymbol{u}_2-\boldsymbol{u}_1), \tag{17.4}$$

$$\alpha_1\frac{\mathrm{D}_1 p_1}{\mathrm{D}t}+\alpha_1\rho_1 a_1^2\mathrm{div}\boldsymbol{u}_1 = \rho_1 a_{1\mathrm{I}}^2\,(\boldsymbol{u}_{\mathrm{I}}-\boldsymbol{u}_1)\cdot\nabla\alpha_1+\mu\rho_1 a_{1\mathrm{I}}^2\,(p_2-p_1)+\frac{\lambda}{\kappa_1\rho_1}(\boldsymbol{u}_{\mathrm{I}}-\boldsymbol{u}_1).(\boldsymbol{u}_2-\boldsymbol{u}_1), \tag{17.5}$$

$$\alpha_2\frac{\mathrm{D}_2 p_2}{\mathrm{D}t}+\alpha_2\rho_2 a_2^2\mathrm{div}\boldsymbol{u}_2 = \rho_2 a_{2\mathrm{I}}^2\,(\boldsymbol{u}_{\mathrm{I}}-\boldsymbol{u}_2)\cdot\nabla\alpha_2-\mu\rho_2 a_{2\mathrm{I}}^2\,(p_2-p_1)-\frac{\lambda}{\kappa_2\rho_2}(\boldsymbol{u}_{\mathrm{I}}-\boldsymbol{u}_2).(\boldsymbol{u}_2-\boldsymbol{u}_1), \tag{17.6}$$

$$\frac{\mathrm{D}_{\mathrm{I}}\alpha_2}{\mathrm{D}t}=\mu(p_2-p_1). \tag{17.7}$$

2.3. Derivation of a reduced model

In this section, to simplify the notation, we present only the one dimensional case or alternatively the expression $A(\boldsymbol{U})\partial\boldsymbol{U}/\partial x$ can be understood as a shorthand notation for $\sum_{j=1}^{d}A_j(\boldsymbol{U})\partial\boldsymbol{U}/\partial x_j$.

The derivation of the model can be presented briefly as follows: Consider an hyperbolic system with stiff source term

$$\frac{\partial\boldsymbol{U}}{\partial t}+A(\boldsymbol{U})\frac{\partial\boldsymbol{U}}{\partial x}=\frac{R(\boldsymbol{U})}{\varepsilon}. \tag{18}$$

In this equation $\boldsymbol{U}=\boldsymbol{U}(x,t)$ the state vector belongs to Ω, some open subset of $\mathbb{R}^{\mathbb{N}}$. We assume that (18) is hyperbolic, i.e., for any $\boldsymbol{U}\in\Omega$, the matrix $A(\boldsymbol{U})$ is diagonalizable in $\mathbb{R}$ and possesses a complete set of eigenvectors.

We are interested in the behavior of the solutions of (18) when the relaxation time ε goes to zero. Therefore, we expect these solutions to be close to $\mathscr{E}$ the subset of $\mathbb{R}^{\mathbb{N}}$ defined by

$$\mathscr{E}=\{\boldsymbol{U}\in\mathbb{R}^{\mathbb{N}};R(\boldsymbol{U})=\mathbb{0}\}. \tag{19}$$

We make the following assumption:

Assumption 1. The set of equations $R(\boldsymbol{U})=0$ defines a smooth manifold of dimension n. Moreover, for any $\boldsymbol{U}\in\mathscr{E}$ we *explicitly* know a parametrization M from ω an open subset of $\mathbb{R}^{\mathbb{n}}$ on V a neighborhood of U in $\mathscr{E}$.

We call $\mathscr{E}$ the equilibrium manifold while in reference to the Boltzmann equation, the smooth diffeomorphism M will be called the "Maxwellian". We note that for any $\boldsymbol{u}\in\omega$ the Jacobian matrix $dM_{\boldsymbol{u}}$ is a full rank matrix. Moreover we have the following result:

Proposition 1. *The column vectors of dM_u form a basis of ker $R'(M(u))$.*

Proof. Denote $T_U(\mathscr{E})$ the tangent space of $\mathscr{E}$ at U. Since M is a diffeomorphism from ω onto $V\subset\mathscr{E}$, dM_u is a bijection from $\mathbb{R}^{\mathbb{n}}$ onto $T_{M(\boldsymbol{u})}(\mathscr{E})$. Therefore the column vectors of dM_u are n independent vectors that form a basis of $T_{M(\boldsymbol{u})}(\mathscr{E})$. But, since the equilibrium manifold $\mathscr{E}$ is defined by the implicit Eqs. (19), the result simply follows by noting that $T_{M(\boldsymbol{u})}(\mathscr{E})$ is precisely ker $R'(M(u))$. □

We will denote the column vectors of $dM_{\boldsymbol{u}}$, $\{dM_{\boldsymbol{u}}^1,\ldots,dM_{\boldsymbol{u}}^n\}$. Now let $\{I^1,\ldots,I^{N-n}\}$ be a basis of $\mathrm{Rng}(R'(M(\boldsymbol{u})))$ the range of $R'(M(\boldsymbol{u}))$ and define the $N\times N$ matrix S by

$$S = [dM_{\boldsymbol{u}}^1, \ldots, dM_{\boldsymbol{u}}^n, I^1, \ldots, I^{N-n}]. \tag{20}$$

Thanks to Poposition 1, S is an invertible matrix. Let us denote by P and Q the $n \times N$ and $N-n \times N$ matrices composed of the first n and last $N-n$ rows respectively of its inverse, we have:

Proposition 2. *Let $ker(R'(M(\boldsymbol{u})))$ and $Rng(R'(M(\boldsymbol{u})))$ be equipped, respectively, with the basis $\{dM_{\boldsymbol{u}}^1, \ldots, dM_{\boldsymbol{u}}^n\}$ and $\{I^1, \ldots, I^{N-n}\}$, then in these basis P and Q are, respectively, the projection on $ker(R'(M(\boldsymbol{u})))$ in the direction of $Rng(R'(M(\boldsymbol{u})))$ and the projection on $Rng(R'(M(\boldsymbol{u})))$ in the direction of $ker(R'(M(\boldsymbol{u})))$.*

Proof. Let $\boldsymbol{v} \in \mathbb{R}^{\mathbb{m}}$, $\mathbf{w} \in \mathbb{R}^{\mathbb{N}-\mathbb{m}}$ and for $\boldsymbol{U} \in \mathbb{R}^{\mathbb{N}}$ let us write: □

$$\boldsymbol{U} = \sum_{j=1}^{n} \boldsymbol{v}^j dM_{\boldsymbol{u}}^j + \sum_{j=1}^{N-n} \boldsymbol{w}^j I^j, \tag{21}$$

then the vectors $\sum_{j=1}^{n} \boldsymbol{v}^j dM_{\mathbf{u}}^j$ and $\sum_{j=1}^{N-n} \mathbf{w}^j I^j$ are clearly, respectively, the projection on $\ker(R'(M(\boldsymbol{u})))$ in the direction of $\mathrm{Rng}(R'(M(\boldsymbol{u})))$ of $\boldsymbol{U}$ and the projection on $\mathrm{Rng}(R'(M(\boldsymbol{u})))$ in the direction of $\ker(R'(M(\boldsymbol{u})))$ of $\boldsymbol{U}$. In matrix form (21) can be written

$$\boldsymbol{U} = S \begin{bmatrix} \boldsymbol{v} \\ \boldsymbol{w} \end{bmatrix} \tag{22}$$

from which we deduce

$$\begin{bmatrix} \boldsymbol{v} \\ \boldsymbol{w} \end{bmatrix} = S^{-1} \boldsymbol{U} = \begin{bmatrix} P\boldsymbol{U} \\ Q\boldsymbol{U} \end{bmatrix}. \tag{23}$$

We note the following simple properties:

Proposition 3. *We have*

1. $P \cdot dM_u = Id(n)$ *where* $Id(n)$ *is the* $n \times n$ *identity matrix*;
2. $P \cdot R'(M(u)) = 0$.

Proof. The first result follows from $S^{-1} \cdot S = Id(N)$. To prove the second result, we note that for any $\boldsymbol{U} \in \mathbb{R}^{\mathbb{m}}$, obviously $R'(M(u))U$ is in the range of $R'(M(u))$. □

Note that Assumption 1 is a very weak one. However, we emphazise that this assumption gives only the possibility to write a *formal* asymptotic expansion. In particular, this weak assumption *does not* imply that the reduced system is well-posed or hyperbolic nor does it implies that the expansion is convergent. More stronger assumptions are needed to establish results of this type. For a survey on some recent results on hyperbolic systems with stiff relaxation terms, the interested reader can see [14].

Now, to obtain a reduced model, we look for a solution in the form

$$\boldsymbol{U} = M(\boldsymbol{u}) + \varepsilon \boldsymbol{V}. \tag{24}$$

Introducing this expression in (18) gives

$$\frac{\partial M(\boldsymbol{u})}{\partial t} + A(M(\boldsymbol{u}))\frac{\partial M(\boldsymbol{u})}{\partial x} - R'(M(\boldsymbol{u}))\cdot \boldsymbol{V} + \varepsilon\left[\frac{\partial \boldsymbol{V}}{\partial t} + A(M(\boldsymbol{u}))\frac{\partial \boldsymbol{V}}{\partial x} + \left[\frac{\partial A}{\partial \boldsymbol{U}_i}\boldsymbol{V}_i\right]\frac{\partial M(\boldsymbol{u})}{\partial x} - \frac{1}{2}R''(M(\boldsymbol{u}))(\boldsymbol{V},\boldsymbol{V})\right] = \mathcal{O}(\varepsilon^2). \tag{25}$$

Thanks to Proposition 3, multiplying this equation by P gives

$$\frac{\partial \boldsymbol{u}}{\partial t} + P\cdot A(M(\boldsymbol{u}))\cdot dM_{\boldsymbol{u}}\frac{\partial \boldsymbol{u}}{\partial x} = \mathcal{O}(\varepsilon). \tag{26}$$

The reduced model of (18) is thus obtained by neglecting the terms of order ε.

2.4. Application to the seven equation model

The application of the previous asymptotic analysis to the seven equation model (17) is straightforward. We just need to identify the Maxwellian $M(\boldsymbol{u})$ and then to compute the Jacobian matrix $dM_{\boldsymbol{u}}$ and the projection matrix P. Let $\mathbf{u} = {}^t(s_1, s_2, u, p, \alpha_2) \in \mathbb{R}^5$ the Maxwellian is defined by

$$\boldsymbol{u} \to \boldsymbol{U} = M(\boldsymbol{u}) = \begin{pmatrix} s_1 \\ s_2 \\ u \\ u \\ p \\ p \\ \alpha_2 \end{pmatrix}.$$

The Jacobian matrix of this transformation is

$$dM_{\boldsymbol{u}} = \begin{pmatrix} 1 & 0 & 0 & 0 & 0 \\ 0 & 1 & 0 & 0 & 0 \\ 0 & 0 & 1 & 0 & 0 \\ 0 & 0 & 1 & 0 & 0 \\ 0 & 0 & 0 & 1 & 0 \\ 0 & 0 & 0 & 1 & 0 \\ 0 & 0 & 0 & 0 & 1 \end{pmatrix}.$$

The linearized source term evaluated on a Maxwellian is

$$R'(M(\boldsymbol{u})) = \begin{pmatrix} 0 & 0 & 0 & 0 & 0 & 0 & 0 \\ 0 & 0 & 0 & 0 & 0 & 0 & 0 \\ 0 & 0 & -1 & 1 & 0 & 0 & 0 \\ 0 & 0 & 1 & -1 & 0 & 0 & 0 \\ 0 & 0 & 0 & 0 & -1 & 1 & 0 \\ 0 & 0 & 0 & 0 & 1 & -1 & 0 \\ 0 & 0 & 0 & 0 & -1 & 1 & 0 \end{pmatrix}.$$

A basis of the range $\mathrm{Rng}(R'(M(\boldsymbol{u})))$ of this matrix is the set

$$I^1 = \begin{pmatrix} 0 \\ 0 \\ -1 \\ 1 \\ 0 \\ 0 \\ 0 \end{pmatrix}, \quad I^2 = \begin{pmatrix} 0 \\ 0 \\ 0 \\ 0 \\ -1 \\ 1 \\ -1 \end{pmatrix}.$$

The inversion of the matrix $S = [dM^1_{\mathbf{u}}, \ldots, dM^5_{\boldsymbol{u}}, I^1, I^2]$ thus gives the projection on $\ker(R'(M(\boldsymbol{u})))$

$$P = \begin{pmatrix} 1 & 0 & 0 & 0 & 0 & 0 & 0 \\ 0 & 1 & 0 & 0 & 0 & 0 & 0 \\ 0 & 0 & 1/2 & 1/2 & 0 & 0 & 0 \\ 0 & 0 & 0 & 0 & 1/2 & 1/2 & 0 \\ 0 & 0 & 0 & 0 & -1/2 & 1/2 & 1 \end{pmatrix}.$$

To obtain, the reduced model, we just need now to compute the matrix product $P \cdot A(M(\boldsymbol{u})) \cdot dM_{\boldsymbol{u}}$. After some straightforward computations, we then get a five equation reduced model written in term of "entropic" variables ${}^t(s_1, s_2, \boldsymbol{u}, p, \alpha_2)$:

$$\frac{\mathrm{D}s_1}{\mathrm{D}t} = 0, \tag{27.1}$$

$$\frac{\mathrm{D}s_2}{\mathrm{D}t} = 0, \tag{27.2}$$

$$\frac{\mathrm{D}\boldsymbol{u}}{\mathrm{D}t} + \frac{1}{\rho}\nabla p = 0, \tag{27.3}$$

$$\frac{\mathrm{D}p}{\mathrm{D}t} + \rho\hat{a}^2 \mathrm{div}\boldsymbol{u} = 0, \tag{27.4}$$

$$\frac{\mathrm{D}\alpha_2}{\mathrm{D}t} = \alpha_1\alpha_2 \frac{\rho_1 a_1^2 - \rho_2 a_2^2}{\sum_{k=1}^2 \alpha_{k'}\rho_k a_k^2} \mathrm{div}\boldsymbol{u}, \tag{27.5}$$

where we have introduced $\mathrm{D}\phi/\mathrm{D}t = \partial\phi/\partial t + \boldsymbol{u}\cdot\nabla\phi$, the mixture density ρ

$$\rho = \sum_{k=1}^{2} \alpha_k \rho_k \tag{28}$$

and also the averaged sound speed $\hat{a}$ defined by the following formula:

$$\frac{1}{\rho\hat{a}^2} = \sum_{k=1}^{2} \frac{\alpha_k}{\rho_k a_k^2}. \tag{29}$$

The relation (29) is known in the two phase flow literature as the Wallis sound speed of the mixture and have been validated by many experiments (see for instance [19] or [6]). Note that system (27) is not new. It is for example described in term of ${}^t(s_1, s_2, \boldsymbol{u}, \rho, Y_2)$ variables in ([19], Section 4.1). With additional mass

transfer terms, this model has been recently tested for detonation studies in [21]. To end this section, we note that after some algebraic manipulations, the model (27) may be written in term of conservative variables ${}^t(\alpha_1\rho_1,\alpha_2\rho_2,\rho\boldsymbol{u},\rho e,\alpha_2)$ as:

$$\frac{\partial \alpha_1\rho_1}{\partial t} + \operatorname{div}(\alpha_1\rho_1\boldsymbol{u}) = 0, \tag{30.1}$$

$$\frac{\partial \alpha_2\rho_2}{\partial t} + \operatorname{div}(\alpha_2\rho_2\boldsymbol{u}) = 0, \tag{30.2}$$

$$\frac{\partial \rho\boldsymbol{u}}{\partial t} + \operatorname{div}(\rho\boldsymbol{u}\otimes\boldsymbol{u}) + \nabla p = 0, \tag{30.3}$$

$$\frac{\partial \rho e}{\partial t} + \operatorname{div}(\rho e + p)\boldsymbol{u} = 0, \tag{30.4}$$

$$\frac{\partial \alpha_2}{\partial t} + \boldsymbol{u}\cdot\nabla\alpha_2 = \alpha_1\alpha_2\frac{\rho_1 a_1^2 - \rho_2 a_2^2}{\sum_{k=1}^{2}\alpha_{k'}\rho_k a_k^2}\operatorname{div}\boldsymbol{u}, \tag{30.5}$$

where e the specific total energy is defined by $e = \varepsilon + \boldsymbol{u}^2/2$ while the specific internal energy ε is given by the relation $\rho\varepsilon = \sum_{k=1}^{2}\alpha_k\rho_k\varepsilon_k(p,\rho_k)$.

Remark. In [2,12], a diffuse interface method for the simulation of interfaces between compressible fluids was introduced. This model (in the sequel referred to as the "five equation-transport model") is very similar to (30) except that instead of (30.5), the equation for the volume fraction is simply a transport equation

$$\frac{\partial \alpha_2}{\partial t} + \boldsymbol{u}\cdot\nabla\alpha_2 = 0. \tag{31}$$

In view of (30.5) and since for interface problems, the zone where the product $\alpha_1\alpha_2$ is expected to be small, the differences between the two models seem unimportant. However, as we will see the mathematical properties of the two models are quite different. In particular, the "five equation-transport model" of [2,12] is not compatible with the fact that the material derivatives of the phase entropies are zero. This is quite obvious from the form (27) of the present reduced model. But it can also be seen as follows: Let us write the equality of the pressures in the two phases

$$p_1(s_1,\rho_1) = p_2(s_2,\rho_2) \tag{32}$$

and take the material derivative of this expression to obtain

$$\left(\frac{\partial p_1}{\partial s_1}\right)_{\rho_1}\frac{\mathrm{D}s_1}{\mathrm{D}t} - \left(\frac{\partial p_2}{\partial s_2}\right)_{\rho_2}\frac{\mathrm{D}s_2}{\mathrm{D}t} = \left(\frac{\partial p_2}{\partial \rho_2}\right)_{s_2}\frac{\mathrm{D}\rho_2}{\mathrm{D}t} - \left(\frac{\partial p_1}{\partial \rho_1}\right)_{s_1}\frac{\mathrm{D}\rho_1}{\mathrm{D}t}. \tag{33}$$

Now, with (30.1) and (30.2) we have

$$\frac{\mathrm{D}\rho_k}{\mathrm{D}t} = \frac{1}{\alpha_k}\left[\frac{D\alpha_k\rho_k}{\mathrm{D}t} - \rho_k\frac{D\alpha_k}{\mathrm{D}t}\right] = -\frac{1}{\alpha_k}\left[\alpha_k\rho_k\operatorname{div}\boldsymbol{u} + \rho_k\frac{D\alpha_k}{\mathrm{D}t}\right] \tag{34}$$

and we get from (33)

$$\left(\frac{\partial p_1}{\partial s_1}\right)_{\rho_1}\frac{\mathrm{D}s_1}{\mathrm{D}t} - \left(\frac{\partial p_2}{\partial s_2}\right)_{\rho_2}\frac{\mathrm{D}s_2}{\mathrm{D}t} + (\rho_1 a_1^2 - \rho_2 a_2^2)\operatorname{div}\boldsymbol{u} = \left(\frac{\rho_2 a_2^2}{\alpha_2} + \frac{\rho_1 a_1^2}{\alpha_1}\right)\frac{\mathrm{D}\alpha_2}{\mathrm{D}t}, \tag{35}$$

that shows that Eq. (30.5) is a direct consequence of the assumptions $Ds_1/Dt = Ds_2/Dt = 0$ and conversely that the assumptions $D\alpha_2/Dt = 0$ is not compatible with these relations. Actually, (35) shows that if $D\alpha_2/Dt = 0$ then the phase entropies must evolve according to the relation

$$\left(\frac{\partial p_1}{\partial s_1}\right)_{\rho_1} \frac{Ds_1}{Dt} - \left(\frac{\partial p_2}{\partial s_2}\right)_{\rho_2} \frac{Ds_2}{Dt} = (\rho_2 a_2^2 - \rho_1 a_1^2)\mathrm{div}\boldsymbol{u}. \tag{36}$$

3. Mathematical study

For regular solutions, the mathematical study of the model can be performed with any set of independent variables. Here, for instance, we will use the set of variables ${}^t(s_1,s_2,\boldsymbol{u},p,Y_2)$ where $Y_k = \alpha_k\rho_k/\rho$ stand for the mass fractions of each phase. It is easily seen from the mass conservation Eqs. (30.1) and (30.2) that Y_k obey the equations $DY_k/Dt = 0$ and the five equation reduced model can be written:

$$\frac{Ds_1}{Dt} = 0, \tag{37.1}$$

$$\frac{Ds_2}{Dt} = 0, \tag{37.2}$$

$$\frac{D\boldsymbol{u}}{Dt} + \frac{1}{\rho}\nabla p = 0, \tag{37.3}$$

$$\frac{Dp}{Dt} + \rho\hat{a}^2\mathrm{div}\boldsymbol{u} = 0, \tag{37.4}$$

$$\frac{DY_2}{Dt} = 0, \tag{37.5}$$

where the mixture density ρ and the averaged sound speed $\hat{a}$ have been defined in the previous Section 2. On the other hand, the system is clearly invariant by rotation. As a consequence for the sake of simplicity, we can perform the mathematical study for the system written in one dimension.

3.1. Hyperbolicity

So if we set $\boldsymbol{q} = {}^t(s_1,s_2,u,p,Y_2)$, for smooth solutions, the system (37) can be written in one dimension as

$$\frac{\partial \boldsymbol{q}}{\partial t} + A(\boldsymbol{q})\frac{\partial \boldsymbol{q}}{\partial x} = 0, \tag{38}$$

where the matrix $A(\boldsymbol{q})$ is defined by

$$A(\boldsymbol{q}) = \begin{pmatrix} u & 0 & 0 & 0 & 0 \\ 0 & u & 0 & 0 & 0 \\ 0 & 0 & u & 1/\rho & 0 \\ 0 & 0 & \rho\hat{a}^2 & u & 0 \\ 0 & 0 & 0 & 0 & u \end{pmatrix}. \tag{39}$$

Since the characteristic equation of $A(\boldsymbol{q})$ is given by $(u-\lambda)^3((u-\lambda)^2 - \hat{a}^2) = 0$, we obtain three distinct eigenvalues for the matrix $A(\boldsymbol{q})$:

$$\begin{cases} \lambda_1(\boldsymbol{q}) = u - \hat{a}, \\ \lambda_2(\boldsymbol{q}) = \lambda_3(\boldsymbol{q}) = \lambda_4(\boldsymbol{q}) = u, \\ \lambda_5(\boldsymbol{q}) = u + \hat{a}, \end{cases} \tag{40}$$

where $\hat{a}$ is given by the relation (29). Thus $\hat{a}$ is clearly real and all the eigenvalues of the matrix $A(\boldsymbol{q})$ are real. The expression (29) where the average "acoustic impedance" $\rho\hat{a}^2$ appears as the harmonic average of the "acoustic impedances" of the pure phases $\rho_k a_k^2$ implies that the sound speed of a mixture can be less than the sound speed of either phase. This fact is well-known in the two-phase literature (see for instance [19] or [6]).

The right eigenvectors $r_i(\boldsymbol{q})$ (for $i \in \{1,\ldots,5\}$) which verify the relation $A(\boldsymbol{q})r_i(\boldsymbol{q}) = \lambda_i(\boldsymbol{q})r_i(\boldsymbol{q})$ can be choosen as:

$$r_1(\boldsymbol{q}) = \begin{pmatrix} 0 \\ 0 \\ \hat{a} \\ -\rho\hat{a}^2 \\ 0 \end{pmatrix}, \quad r_2(\boldsymbol{q}) = \begin{pmatrix} 1 \\ 0 \\ 0 \\ 0 \\ 0 \end{pmatrix}, \quad r_3(\boldsymbol{q}) = \begin{pmatrix} 0 \\ 1 \\ 0 \\ 0 \\ 0 \end{pmatrix}, \quad r_4(\boldsymbol{q}) = \begin{pmatrix} 0 \\ 0 \\ 0 \\ 0 \\ 1 \end{pmatrix}, \quad r_5(\boldsymbol{q}) = \begin{pmatrix} 0 \\ 0 \\ \hat{a} \\ \rho\hat{a}^2 \\ 0 \end{pmatrix}. \tag{41}$$

We denote also by $l_i(\boldsymbol{q})$ (for $i \in \{1,\ldots,5\}$) the left eigenvectors which obey the relation ${}^t A(\boldsymbol{q})l_i(\boldsymbol{q}) = \lambda_i(\boldsymbol{q})l_i(\boldsymbol{q})$. After normalization of the left and right eigenvectors to have ${}^t l_i(\boldsymbol{q}) \cdot r_j(\boldsymbol{q}) = \delta_{ij}$, we get:

$$l_1(\boldsymbol{q}) = \begin{pmatrix} 0 \\ 0 \\ 1/2\hat{a} \\ -1/2\rho\hat{a}^2 \\ 0 \end{pmatrix}, \quad l_2(\boldsymbol{q}) = \begin{pmatrix} 1 \\ 0 \\ 0 \\ 0 \\ 0 \end{pmatrix}, \quad l_3(\boldsymbol{q}) = \begin{pmatrix} 0 \\ 1 \\ 0 \\ 0 \\ 0 \end{pmatrix}, \quad l_4(\boldsymbol{q}) = \begin{pmatrix} 0 \\ 0 \\ 0 \\ 0 \\ 1 \end{pmatrix}, \quad l_5(\boldsymbol{q}) = \begin{pmatrix} 0 \\ 0 \\ 1/2\hat{a} \\ 1/2\rho\hat{a}^2 \\ 0 \end{pmatrix}. \tag{42}$$

The system is thus clearly hyberbolic since the matrix $A(\boldsymbol{q})$ is diagonalizable in $\mathbb{R}$ and its eigenvectors span the whole space $\mathbb{R}^5$. We note that this system is unconditionally hyperbolic as soon as the sound speed in the pure fluids are real whatever the state laws of the pure fluids are.

Remark. In the "five equation-transport model" of [2,12], the sound speed is given by the expression

$$\xi\hat{a}^2 = \sum_{k=1}^{2} \xi_k Y_k a_k^2, \tag{43}$$

where $\xi_k = (\partial\rho_k\varepsilon_k/\partial p_k)_{\rho_k}$ and $\xi = \sum_{k=1}^{2}\alpha_k\xi_k$. Thus as in (29), the sound speed of the mixture appears as some average of the phase sound speeds. However, these averages are different in the two models. In some extreme cases, for real fluids the coefficients ξ_k can be negative and the formula (43) does not guarantee that the mixture speed of sound is real while formula (29) will always yield a real speed of sound.

Fig. 1 displays the sound speed of an air–water mixture with respect to the air volume fraction, under atmospheric conditions, respectively for the five equation reduced model and the "five equation-transport model". One can notice that the values of the sound speeds are very different in the two models. In particular, the sound speed given by (43) is always larger than the Wallis sound speed (29). Moreover it is strictly between the sound speed of the pure fluids in contrast with the Wallis sound speed that is generally lower

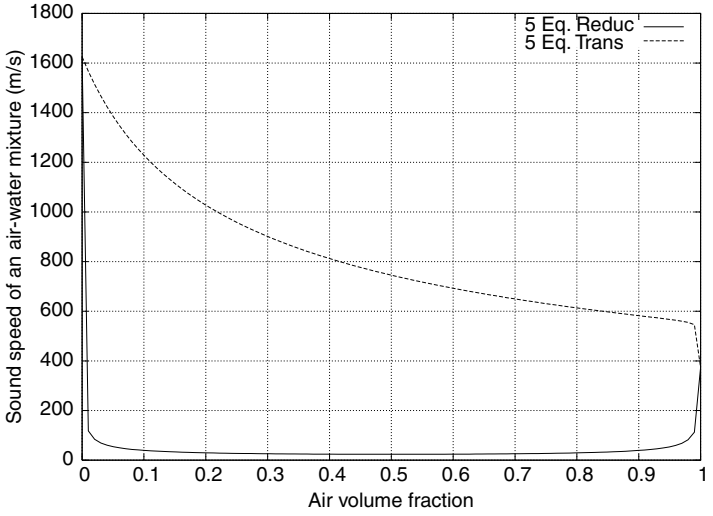

Fig. 1. Sound speed of an air–water mixture under atmospheric conditions for the 5 equation reduced model (solid line) and the 5 equation transport model (dotted line).

than the sound speed of the pure fluids. For interface computations with adequate resolution, it is possible that these differences are insignificant, however if the zones of numerical diffusion are not negligeable, these differences can shown up on the macroscopic level.

3.2. Existence of a mathematical entropy

Since the phase entropies s_1, s_2 satisfy (37.1) and (37.2), the existence of an entropy for the five equation reduced system is obvious. The simplest choice is to define S by

$$\rho S = \alpha_1\rho_1 s_1 + \alpha_2\rho_2 s_2 = \rho Y_1 s_1 + \rho Y_2 s_2 \tag{44}$$

and we have

$$\frac{\partial \rho S}{\partial t} + \operatorname{div}(\rho S \boldsymbol{u}) = 0. \tag{45}$$

3.3. Structure of the waves

In this section, we analyze the structure of the waves. The objective is to show that the system contains fields which are either genuinely non linear or linearly degenerate (see for instance [7]). So let us start with the characteristic fields associated to the waves $u - \hat{a}$ and $u + \hat{a}$.

Proposition 4. *The characteristic fields associated to the waves* $\lambda_1(\boldsymbol{q}) = u - \hat{a}$ *and* $\lambda_5(\boldsymbol{q}) = u + \hat{a}$ *are genuinely non linear, i.e., we have* $\nabla_{\boldsymbol{q}}\lambda_1(\boldsymbol{q}) \cdot r_1(\boldsymbol{q}) \neq 0$ *and* $\nabla_{\boldsymbol{q}}\lambda_5(\boldsymbol{q}) \cdot r_5(\boldsymbol{q}) \neq 0$ *for all admissible state vector* $\boldsymbol{q}$.

Proof. We can deduce from the eigenvalues (40) and the right eigenvectors (41) the relation

$$\nabla_{\boldsymbol{q}}\lambda_1(\boldsymbol{q}) \cdot r_1(\boldsymbol{q}) = \nabla_{\boldsymbol{q}}\lambda_5(\boldsymbol{q}) \cdot r_5(\boldsymbol{q}) = \hat{a} + \rho\hat{a}^2 \frac{\partial \hat{a}}{\partial p}. \tag{46}$$

So the proof consists to show that $\hat{a} + \rho\hat{a}^2\partial\hat{a}/\partial p$ is always non zero and the principal difficulty is to evaluate the term $\partial\hat{a}/\partial p$. Let us first rewrite, in term of the mass fractions Y_k, the mixture density (28) as

$$\frac{1}{\rho} = \sum_{k=1}^{2} \frac{Y_k}{\rho_k} \tag{47}$$

and also the averaged sound speed (29) under the form

$$\frac{1}{(\rho\hat{a})^2} = \sum_{k=1}^{2} \frac{Y_k}{(\rho_k a_k)^2}. \tag{48}$$

Now let us consider the following differentiation of the sound speed $\hat{a}$ for an arbitrary variable ϕ

$$\frac{\partial\hat{a}}{\partial\phi} = -\hat{a}\left[\frac{(\rho\hat{a})^2}{2}\frac{\partial}{\partial\phi}\left(\frac{1}{(\rho\hat{a})^2}\right) - \rho\frac{\partial}{\partial\phi}\left(\frac{1}{\rho}\right)\right]. \tag{49}$$

Using this relation (49) for $\phi = p$ and introducing expressions (47) and (48) we get:

$$\begin{aligned}
\hat{a} + \rho\hat{a}^2\frac{\partial\hat{a}}{\partial p} &= \hat{a} - \rho\hat{a}^3\left[\frac{(\rho\hat{a})^2}{2}\frac{\partial}{\partial p}\left(\sum_{k=1}^{2}\frac{Y_k}{(\rho_k a_k)^2}\right) - \rho\frac{\partial}{\partial p}\left(\sum_{k=1}^{2}\frac{Y_k}{\rho_k}\right)\right],\\
\hat{a} + \rho\hat{a}^2\frac{\partial\hat{a}}{\partial p} &= \hat{a} - \rho\hat{a}^3\left[\frac{(\rho\hat{a})^2}{2}\sum_{k=1}^{2}Y_k\frac{\partial}{\partial p}\left(\frac{1}{(\rho_k a_k)^2}\right) - \rho\sum_{k=1}^{2}Y_k\frac{\partial}{\partial p}\left(\frac{1}{\rho_k}\right)\right].
\end{aligned} \tag{50}$$

Then introducing the coefficients $\psi_k = (\partial a_k/\partial p_k)_{s_k}$ for each phase and recalling that the definition of the phase sound speeds implies $(\partial\rho_k/\partial p_k)_{s_k} = 1/a_k^2$, we obtain the following results:

$$\begin{aligned}
\hat{a} + \rho\hat{a}^2\frac{\partial\hat{a}}{\partial p} &= \hat{a} - \rho\hat{a}^3\left[-(\rho\hat{a})^2\sum_{k=1}^{2}\frac{Y_k(1+\rho_k a_k\psi_k)}{\rho_k^3 a_k^4} + \rho\sum_{k=1}^{2}\frac{Y_k}{(\rho_k a_k)^2}\right],\\
\hat{a} + \rho\hat{a}^2\frac{\partial\hat{a}}{\partial p} &= \hat{a} - \rho\hat{a}^3\left[-(\rho\hat{a})^2\sum_{k=1}^{2}\frac{Y_k(1+\rho_k a_k\psi_k)}{\rho_k^3 a_k^4} + \frac{1}{\rho\hat{a}^2}\right],
\end{aligned} \tag{51}$$

which give us after simplifications:

$$\hat{a} + \rho\hat{a}^2\frac{\partial\hat{a}}{\partial p} = \rho^3\hat{a}^5\sum_{k=1}^{2}\frac{Y_k(1+\rho_k a_k\psi_k)}{\rho_k^3 a_k^4}. \tag{52}$$

And finally assuming that $\psi_k > 0$, i.e., the phase sound speed increases with the pressure, when the entropy is constant, we get $(1 + \rho_k a_k\psi_k) \neq 0$ and this achieve the proof. □

Remark. We note that if the fluids are governed by the Stiffened–Gas equation of state; the condition $\psi_k > 0$ is equivalent to $\gamma_k > 1$ where γ_k denotes the adiabatic exponent of each phase.

Now let us examine the characteristic field associated to the wave u.

Proposition 5. *The characteristic field associated to the wave $\lambda_2(\boldsymbol{q}) = \lambda_3(\boldsymbol{q}) = \lambda_4(\boldsymbol{q}) = u$ is linearly degenerate, i.e., we have: $\nabla_{\boldsymbol{q}}\lambda_i(\boldsymbol{q})\cdot r_i(\boldsymbol{q}) = 0$ (for $i \in \{2,3,4\}$) for all admissible state vector $\boldsymbol{q}$.*

Proof. We deduce from the eigenvalues (40) the relation

$$\nabla_{\boldsymbol{q}}\lambda_i(\boldsymbol{q})\cdot r_i(\boldsymbol{q}) = (0,0,1,0,0)\cdot r_i(\boldsymbol{q}) \quad \text{for } i \in \{2,3,4\}. \tag{53}$$

Then introducing the right eigenvectors (41) in the relation (53), it is easily checked that $\nabla_{\boldsymbol{q}}\lambda_i(\boldsymbol{q})\cdot r_i(\boldsymbol{q})=0$ (for $i\in\{2,3,4\}$) and this complete the proof. □

3.4. Riemann's invariants

In this section we compute the Riemann's invariants of the system. Let us begin with the Riemann's invariants ω associated to the eigenvalue $\lambda_1(\mathbf{q})=u-\hat{a}$. The problem is thus to find ω such as $\nabla_{\boldsymbol{q}}\omega\cdot r_1(\boldsymbol{q})=0$. So if we search ω such that $\nabla_{\boldsymbol{q}}\omega$ is collinear with ${}^t l_2(\boldsymbol{q})$, ${}^t l_3(\boldsymbol{q})$ and ${}^t l_4(\boldsymbol{q})$, it is easily checked that s_1, s_2 and Y_2 are three Riemann's invariants associated to this wave. Now if we search $\nabla_{\boldsymbol{q}}\omega$ collinear with ${}^t(2\hat{a}l_5)=(0,0,1,1/\rho\hat{a},0)$, we get the last Riemann's invariant

$$u+\int_p\frac{\mathrm{d}p}{\rho\hat{a}}.$$

We note that this last expression for ω is formally equivalent to the well-known expression of the Riemann's invariant $u+2a/(\gamma-1)$ of the Euler equations of gas dynamics. To summarize, the Riemann's invariants associated to the wave $u-\hat{a}$ are defined by

$$\left\{s_1,s_2,Y_2,u+\int_p\frac{\mathrm{d}p}{\rho\hat{a}}\right\}. \tag{54}$$

After similar algebraic manipulations, it is easily checked that the Riemann's invariants associated to the wave $u+\hat{a}$ are defined by

$$\left\{s_1,s_2,Y_2,u-\int_p\frac{\mathrm{d}p}{\rho\hat{a}}\right\}. \tag{55}$$

On the other hand, the Riemann's invariants associated to the wave u are given by

$$\{u,p\}. \tag{56}$$

To close this section, we also note that if the system is written in term of conservative variables, the first four equations of (30) are in conservative form and give us a set of 4 jump conditions that discontinuities have to satisfy:

$$\Delta[\alpha_1\rho_1(u-\sigma)]=0, \tag{57.1}$$

$$\Delta[\alpha_2\rho_2(u-\sigma)]=0, \tag{57.2}$$

$$\Delta[\rho u(u-\sigma)+p]=0, \tag{57.3}$$

$$\Delta[\rho e(u-\sigma)+pu]=0 \tag{57.4}$$

with $\Delta\phi=\phi_{\mathrm{R}}-\phi_{\mathrm{L}}$ and σ the velocity of the discontinuity. However, the equation for the volume fraction α_2 is not in conservative form and therefore, the system must be supplemented or regularized to specify the admissible shock waves. As discussed in [9], such a regularization can be obtained by a close examination of the structure of the large gradient relaxation zones or by a construction of subscale models of the physical processes occurring within the discontinuities. However, it is doubtful that an universal jump relation can hold. Thus, in the absence of any informations on the micro-physics occurring inside the shock zone, we had to adopt a simpler approach and to rely on artificial viscosity to regularize the model.

4. Numerical approximation

4.1. The VFRoe-ncv scheme

In this section, we describe a quasi-conservative finite volume scheme. The method is based on VFRoe-ncv type scheme [4], i.e., on the solution of a linearized Riemann's problem at each interface of the mesh. Consider the following linearized Riemann's problem between the states $(.)_L$ and $(.)_R$:

$$\begin{cases} \frac{\partial \boldsymbol{q}}{\partial t} + A(\langle \boldsymbol{q} \rangle)\frac{\partial \boldsymbol{q}}{\partial x} = 0, \\ \boldsymbol{q}(x,0) = \begin{vmatrix} \boldsymbol{q}_L & \text{if } x < 0, \\ \boldsymbol{q}_R & \text{if } x > 0. \end{vmatrix} \end{cases} \tag{58}$$

Here, we use the set of variables $\boldsymbol{q} = {}^t(s_1,s_2,v_n,v_t,p,Y_2)$, where v_n, v_t are, respectively, the two components of the vector velocity in the local basis $(\boldsymbol{\eta}_{LR}, \boldsymbol{\eta}^{\perp}_{LR})$ where $\boldsymbol{\eta}_{LR}$ is the unit normal vector to the interface. We define $A(\langle \boldsymbol{q} \rangle)$ by

$$A(\langle \boldsymbol{q} \rangle) = \begin{pmatrix} \langle v_n \rangle & 0 & 0 & 0 & 0 & 0 \\ 0 & \langle v_n \rangle & 0 & 0 & 0 & 0 \\ 0 & 0 & \langle v_n \rangle & 0 & \langle 1/\rho \rangle & 0 \\ 0 & 0 & 0 & \langle v_n \rangle & 0 & 0 \\ 0 & 0 & \langle \rho \hat{a}^2 \rangle & 0 & \langle v_n \rangle & 0 \\ 0 & 0 & 0 & 0 & 0 & \langle v_n \rangle \end{pmatrix}, \tag{59}$$

where $\langle . \rangle = ((.)_L + (.)_R)/2$ denotes the arithmetic average between the states $(.)_L$ and $(.)_R$. Section 3.1 shows that the matrix $A(\langle \boldsymbol{q} \rangle)$ is diagonalizable and the solution procedure reduces to the solving of a Riemann's problem for a linear hyperbolic system.

We denote by $r_i(\langle \boldsymbol{q} \rangle)$ (for $i \in \{1,\ldots,6\}$) the right eigenvectors and by $l_i(\langle \boldsymbol{q} \rangle)$ (for $i \in \{1,\ldots,6\}$) the left eigenvectors of the matrix $A(\langle \boldsymbol{q} \rangle)$, satisfying ${}^t l_i(\langle \boldsymbol{q} \rangle) \cdot r_j(\langle \boldsymbol{q} \rangle) = \delta_{ij}$. The solution of the problem which depends only to the variable x/t is composed, in the (x,t) plane, of constant states separated by characteristic lines. Here we are interested by the solution at the interface, i.e., on $x/t = 0$.

The approximate state at the interface, noted here $\mathbf{q}^*_{LR}$, is given by

$$\boldsymbol{q}^*_{LR} = \boldsymbol{q}\left(\frac{x}{t} = 0, \boldsymbol{q}_L, \boldsymbol{q}_R\right) = \begin{cases} \boldsymbol{q}_L + \sum\limits_{\lambda_i < 0} {}^t l_i(\langle \boldsymbol{q} \rangle) \cdot (\boldsymbol{q}_R - \boldsymbol{q}_L) r_i(\langle \boldsymbol{q} \rangle) \\ \boldsymbol{q}_R - \sum\limits_{\lambda_i > 0} {}^t l_i(\langle \boldsymbol{q} \rangle) \cdot (\boldsymbol{q}_R - \boldsymbol{q}_L) r_i(\langle \boldsymbol{q} \rangle) \end{cases}. \tag{60}$$

In the sequel we will denote by $\boldsymbol{Q} = {}^t(\alpha_1\rho_1,\alpha_2\rho_2,\rho u,\rho v,\rho e,\alpha_2)$ the set of conservative variables where u,v are the two-components of the vector velocity $\boldsymbol{u}$ in the global basis corresponding to the vector $\boldsymbol{q}$ written in entropy variables ${}^t(s_1,s_2,v_n,v_t,p,Y_2)$. In particular $\boldsymbol{Q}^*_{LR}$ will represent the solution of the linearized Riemann's problem (58) written in conservative variables.

To deal with the non-conservative equation

$$\frac{\partial \alpha_2}{\partial t} + \boldsymbol{u} \cdot \nabla \alpha_2 = \alpha_1 \alpha_2 \frac{\rho_1 a_1^2 - \rho_2 a_2^2}{\sum_{k=1}^{2} \alpha_{k'} \rho_k a_k^2} \mathrm{div} \boldsymbol{u}, \tag{61}$$

we re-write it under the form

$$\frac{\partial \alpha_2}{\partial t} + \mathrm{div}(\alpha_2 \boldsymbol{u}) + B(\boldsymbol{Q}) \mathrm{div} \boldsymbol{u} = 0 \quad \text{with} \quad B(\boldsymbol{Q}) = \frac{-\alpha_2 \rho_1 a_1^2}{\sum_{k=1}^{2} \alpha_{k'} \rho_k a_k^2} \tag{62}$$

and we write the five equation reduced model as

$$\frac{\partial \boldsymbol{Q}}{\partial t} + \mathrm{div}\boldsymbol{F}(\boldsymbol{Q}) + \mathrm{div}\boldsymbol{u}\boldsymbol{B}(\boldsymbol{Q}) = 0, \tag{63}$$

where the vector $\boldsymbol{B}(\boldsymbol{Q}) = {}^t(0,0,0,0,0,B(\boldsymbol{Q}))$. Integrating this equation on a cell C_i gives

$$A_i \frac{\partial \boldsymbol{Q}_i}{\partial t} + \int_{\partial C_i} \boldsymbol{F}(\boldsymbol{Q}) \cdot \boldsymbol{n}\,\mathrm{d}l + \int_{C_i} \boldsymbol{B}(\boldsymbol{Q})\mathrm{div}\boldsymbol{u}\,\mathrm{d}\Omega = 0 \quad \text{for } i \in \{1,\ldots,N\}, \tag{64}$$

where N is the number of cells and A_i the area of the cell C_i. Then we update variables $\boldsymbol{Q}_i$ by the following expression:

$$A_i \frac{\boldsymbol{Q}_i^{n+1} - \boldsymbol{Q}_i^n}{\Delta t} + \sum_{j \in v(i)} \|\boldsymbol{n}_{ij}\| \boldsymbol{\psi}(\boldsymbol{Q}_i^n, \boldsymbol{Q}_j^n) = 0, \tag{65}$$

where $v(i)$ denote the set of cells C_j that share an edge with C_i and where $\boldsymbol{n}_{ij} = \int_{\partial C_{ij}} \boldsymbol{n}\,\mathrm{d}l$ is the averaged normal vector of the interface $\partial C_{ij} = \partial C_i \cap \partial C_j$. Defining $\boldsymbol{\eta}_{ij} = \boldsymbol{n}_{ij}/\|\boldsymbol{n}_{ij}\|$ and:

$$(v_n)_{ij} = \boldsymbol{u}_{ij} \cdot \boldsymbol{\eta}_{ij} = u_{ij}\eta_{ij}^x + v_{ij}\eta_{ij}^y, \tag{66.1}$$

$$(v_t)_{ij} = \boldsymbol{u}_{ij} \cdot \boldsymbol{\eta}_{ij}^{\perp} = -u_{ij}\eta_{ij}^y + v_{ij}\eta_{ij}^x, \tag{66.2}$$

the normal and tangential components of the velocity at the cell interface, we propose the following expression for $\boldsymbol{\psi}(\boldsymbol{Q}_i^n, \boldsymbol{Q}_j^n)$:

$$\boldsymbol{\psi}(\boldsymbol{Q}_i^n, \boldsymbol{Q}_j^n) = \boldsymbol{F}(\boldsymbol{Q}_{ij}^*) \cdot \boldsymbol{\eta}_{ij} + \boldsymbol{B}(\boldsymbol{Q}_i^n)\boldsymbol{u}_{ij}^* \cdot \boldsymbol{\eta}_{ij}, \tag{67}$$

where $\boldsymbol{Q}_{ij}^*$ is the solution (60) of the linearized Riemann's problem between the states $(.)_i$ and $(.)_j$.

The conservative part $\boldsymbol{F}(\boldsymbol{Q}_{ij}^*) \cdot \boldsymbol{\eta}_{ij}$ can be explicitly written

$$\boldsymbol{F}(\boldsymbol{Q}_{ij}^*).\boldsymbol{\eta}_{ij} = {}^t((\alpha_1\rho_1 v_n)_{ij}^*, (\alpha_2\rho_2 v_n)_{ij}^*, (\rho u v_n)_{ij}^* + p_{ij}^*\eta_{ij}^x, (\rho v v_n)_{ij}^* + p_{ij}^*\eta_{ij}^y, ((\rho e + p)v_n)_{ij}^*, (\alpha_2 v_n)_{ij}^*), \tag{68}$$

while the non-conservative part $\boldsymbol{B}(\boldsymbol{Q}_i^n)\boldsymbol{u}_{ij}^*.\boldsymbol{\eta}_{ij}$ is defined by

$$\boldsymbol{B}(\boldsymbol{Q}_i^n)\boldsymbol{u}_{ij}^* \cdot \boldsymbol{\eta}_{ij} = {}^t(0,0,0,0,0,B(\boldsymbol{Q}_i^n)(v_n)_{ij}^*). \tag{69}$$

4.2. Evolution of a contact discontinuity

As shown in [17], one key point for the simulation of interface problems between compressible fluid is the capability of the scheme to compute an isolated contact discontinuity without pressure oscillations. In the following, we thus study the capability of the scheme to preserve a uniform pressure and velocity flow. Consider an initial flow where pressure and velocity have uniform values; $u_{i-1} = u_i = u_{i+1} = u$ and $p_{i-1} = p_i = p_{i+1} = p$ but other quantities $\alpha_k\rho_k,\alpha_2$ can be discontinuous. We denote by $\boldsymbol{Q}_{i-1},\boldsymbol{Q}_i,\boldsymbol{Q}_{i+1}$ the conservative variables vectors. Then if we suppose for instance $u > 0$, it is easily seen that the solution of the linearized Riemann's problem at each interface is given by:

$$\begin{cases} \boldsymbol{Q}_{i-1/2}^* = \boldsymbol{Q}_{i-1}, \\ \boldsymbol{Q}_{i+1/2}^* = \boldsymbol{Q}_i, \\ \boldsymbol{Q}_{i+3/2}^* = \boldsymbol{Q}_{i+1}. \end{cases} \tag{70}$$

And thus the only cell whose value is changed between t and $t + \Delta t$ is the cell downstream of the discontinuity. The value of $\boldsymbol{Q}$ in this cell becomes:

$$\begin{aligned}
\boldsymbol{Q}_{i+1}^{n+1} &= \boldsymbol{Q}_{i+1}^{n} - \lambda(\boldsymbol{F}(\boldsymbol{Q}_{i+3/2}^{*}) - \boldsymbol{F}(\boldsymbol{Q}_{i+1/2}^{*})) - \lambda \boldsymbol{B}(\boldsymbol{Q}_{i+1}^{n})(u_{i+3/2}^{*} - u_{i+1/2}^{*}),\\
\boldsymbol{Q}_{i+1}^{n+1} &= \boldsymbol{Q}_{i+1}^{n} - \lambda(\boldsymbol{F}(\boldsymbol{Q}_{i+1}) - \boldsymbol{F}(\boldsymbol{Q}_{i})) - \lambda \boldsymbol{B}(\boldsymbol{Q}_{i+1}^{n})(u_{i+1} - u_{i}),\\
\boldsymbol{Q}_{i+1}^{n+1} &= \boldsymbol{Q}_{i+1}^{n} - \lambda(\boldsymbol{F}(\boldsymbol{Q}_{i+1}) - \boldsymbol{F}(\boldsymbol{Q}_{i}))
\end{aligned} \tag{71}$$

with $\lambda = \Delta t/A_i$. So the mass conservation equations can be written

$$(\alpha_k \rho_k)_{i+1}^{n+1} = (\alpha_k \rho_k)_{i+1}^{n} - \lambda u[(\alpha_k \rho_k)_{i+1}^{n} - (\alpha_k \rho_k)_{i}^{n}] \quad \text{for } k = 1, 2. \tag{72}$$

And we get for the evolution of the mixture density $\rho = \sum_{k=1}^{2} \alpha_k \rho_k$

$$\rho_{i+1}^{n+1} = \rho_{i+1}^{n} - \lambda u[\rho_{i+1}^{n} - \rho_{i}^{n}]. \tag{73}$$

Now if we look at the momentum conservation equation, we have:

$$\begin{aligned}
(\rho u)_{i+1}^{n+1} &= (\rho u)_{i+1}^{n} - \lambda[\rho_{i+1}^{n} u^2 + p - \rho_{i}^{n} u^2 + p],\\
(\rho u)_{i+1}^{n+1} &= (\rho u)_{i+1}^{n} - \lambda u^2[\rho_{i+1}^{n} - \rho_{i}^{n}],
\end{aligned} \tag{74}$$

that together with (73) gives

$$u_{i+1}^{n+1} = u_{i+1}^{n} = u. \tag{75}$$

Then the total energy equation is written

$$(\rho e)_{i+1}^{n+1} = (\rho e)_{i+1}^{n} - \lambda u[(\rho e)_{i+1}^{n} - (\rho e)_{i}^{n}]. \tag{76}$$

Using the equation for the mixture density (73) and the result $u_{i+1}^{n+1} = u_{i+1}^{n} = u$, we get (where ε stands for the internal mixture energy)

$$(\rho \varepsilon)_{i+1}^{n+1} = (\rho \varepsilon)_{i+1}^{n} - \lambda u[(\rho \varepsilon)_{i+1}^{n} - (\rho \varepsilon)_{i}^{n}]. \tag{77}$$

Then using the Stiffened–Gas state law for each phase, we have the following expression for the mixture internal energy:

$$\rho \varepsilon = \sum_{k=1}^{2} \alpha_k \frac{p + \gamma_k \pi_k}{\gamma_k - 1}. \tag{78}$$

Solving for the pressure with the volume fraction equation

$$(\alpha_2)_{i+1}^{n+1} = (\alpha_2)_{i+1}^{n} - \lambda u[(\alpha_2)_{i+1}^{n} - (\alpha_2)_{i}^{n}]. \tag{79}$$

We get

$$p_{i+1}^{n+1} = p_{i+1}^{n} = p. \tag{80}$$

Therefore, this result guarantee that a contact discontinuity will remain at constant velocity and pressure (although it will evolve toward a smeared profile due to the numerical diffusion).

4.3. Acoustic solver

The results of the previous section show that the VFRoe-ncv scheme preserve an isolated contact discontinuity and that the velocity and the pressure must stay constant in this case. Numerical experiment confirm that this is indeed the case *except* at very low Mach number. This seems surprising because the previous proof is independent of the Mach number. However, this proof assumes that the computations are done with *exact* arithmetic. In practice, this is not the case and round-off errors perturbate the computations. In [13] a close examination of this problem was done and has shown that the

computation of the interface pressure in Eq. (60) is extremely sensible to round-off errors at small Mach number. This is the reason why we have developed another approximate Riemann solver where the computation of the pressure appear to be less sensible to small random perturbations. This second numerical scheme uses more heavily the mathematical structure of the reduced system. It can be understood as an extension of the acoustic solver described for instance in [20] for the Euler equations of gas dynamics. With respect to the different numerical test, this acoustic solver seems to be very robust with respect to the Mach number and specially for interface problems. The principle of this solver is to write linearized characteristic equations starting on the two side of the discontinuity and to compute their intersection to get the velocity and pressure at the interface. To be more specific we first transform the system of partial differential equations into ordinary differential equations by multiply them with the left eigenvectors

$$ {}^t l_i(\boldsymbol{q}) \cdot \left(\frac{\partial \boldsymbol{q}}{\partial t} + A(\boldsymbol{q}) \frac{\partial \boldsymbol{q}}{\partial x} \right) = 0, \tag{81} $$

which can be immediately rewritten

$$ {}^t l_i(\boldsymbol{q}) \cdot \left(\frac{\partial \boldsymbol{q}}{\partial t} + \lambda_i(\boldsymbol{q}) \frac{\partial \boldsymbol{q}}{\partial x} \right) = 0. \tag{82} $$

Now, denoting $q_{\mathrm{L}}^*, q_{\mathrm{R}}^*$, respectively, the states on the left and right side of the contact discontinuity and linearizing (82) with respect to q_{L} and q_{R} we get

$$ \begin{cases} {}^t l_5(\boldsymbol{q}_{\mathrm{L}}) \cdot (\boldsymbol{q}_{\mathrm{L}}^* - \boldsymbol{q}_{\mathrm{L}}) = 0, \\ {}^t l_1(\boldsymbol{q}_{\mathrm{R}}) \cdot (\boldsymbol{q}_{\mathrm{R}}^* - \boldsymbol{q}_{\mathrm{R}}) = 0, \end{cases} \tag{83} $$

which gives after some algebraic manipulations

$$ \begin{cases} \rho_{\mathrm{L}} \hat{a}_{\mathrm{L}} (u_{\mathrm{L}}^* - u_{\mathrm{L}}) + (p_{\mathrm{L}}^* - p_{\mathrm{L}}) = 0, \\ \rho_{\mathrm{R}} \hat{a}_{\mathrm{R}} (u_{\mathrm{R}}^* - u_{\mathrm{R}}) - (p_{\mathrm{R}}^* - p_{\mathrm{R}}) = 0. \end{cases} \tag{84} $$

Then using the fact that $u_{\mathrm{L}}^* = u_{\mathrm{R}}^* = u^*$ and $p_{\mathrm{L}}^* = p_{\mathrm{R}}^* = p^*$, we get the following expressions for u^* and p^*:

$$ \begin{cases} u^* = \frac{\rho_{\mathrm{L}} \hat{a}_{\mathrm{L}} u_{\mathrm{L}} + \rho_{\mathrm{R}} \hat{a}_{\mathrm{R}} u_{\mathrm{R}}}{\rho_{\mathrm{L}} \hat{a}_{\mathrm{L}} + \rho_{\mathrm{R}} \hat{a}_{\mathrm{R}}} - \frac{p_{\mathrm{R}} - p_{\mathrm{L}}}{\rho_{\mathrm{L}} \hat{a}_{\mathrm{L}} + \rho_{\mathrm{R}} \hat{a}_{\mathrm{R}}}, \\ p^* = \frac{\rho_{\mathrm{R}} \hat{a}_{\mathrm{R}} p_{\mathrm{L}} + \rho_{\mathrm{L}} \hat{a}_{\mathrm{L}} p_{\mathrm{R}}}{\rho_{\mathrm{L}} \hat{a}_{\mathrm{L}} + \rho_{\mathrm{R}} \hat{a}_{\mathrm{R}}} - \frac{\rho_{\mathrm{L}} \hat{a}_{\mathrm{L}} \rho_{\mathrm{R}} \hat{a}_{\mathrm{R}} (u_{\mathrm{R}} - u_{\mathrm{L}})}{\rho_{\mathrm{L}} \hat{a}_{\mathrm{L}} + \rho_{\mathrm{R}} \hat{a}_{\mathrm{R}}}. \end{cases} \tag{85} $$

And finally the solution of the Riemann's problem is given by

$$ \boldsymbol{q}\left(\tfrac{x}{t}, \boldsymbol{q}_{\mathrm{L}}, \boldsymbol{q}_{\mathrm{R}}\right) = \begin{cases} \boldsymbol{q}_{\mathrm{L}} & \text{if } \frac{x}{t} < u_{\mathrm{L}} - \hat{a}_{\mathrm{L}}, \\ \boldsymbol{q}_{\mathrm{L}}^* & \text{if } u_{\mathrm{L}} - \hat{a}_{\mathrm{L}} < \frac{x}{t} < u^*, \\ \boldsymbol{q}_{\mathrm{R}}^* & \text{if } u^* < \frac{x}{t} < u_{\mathrm{R}} + \hat{a}_{\mathrm{R}}, \\ \boldsymbol{q}_{\mathrm{R}} & \text{if } u_{\mathrm{R}} + \hat{a}_{\mathrm{R}} < \frac{x}{t}. \end{cases} \tag{86} $$

The same numerical scheme which has been presented in Section 4.1 can be used with this Riemann solver. We also note that as shown in expression (85), in an isolated contact discontinuity with $p_{\mathrm{L}} = p_{\mathrm{R}}$ and $u_{\mathrm{L}} = u_{\mathrm{R}}$ the interface values of the velocity and pressure will again have this common value. The results of Section (4.2) thus remain valid when this approximate Riemann solver is used.

5. Numerical results

5.1. Multifluid/interface problems: validation tests

5.1.1. Pure interface advection

This first validation test is a one dimension interface advection between water and air. The state laws for the air and the water are given by the Stiffened–Gas formulation:

$$p = (\gamma_1 - 1)\rho_1\varepsilon_1 - \gamma_1\pi_1 \quad \text{with } \gamma_1 = 1.4 \quad \text{and} \quad \pi_1 = 0 \text{ air}, \tag{87.1}$$

$$p = (\gamma_2 - 1)\rho_2\varepsilon_2 - \gamma_2\pi_2 \quad \text{with } \gamma_2 = 4.4 \quad \text{and} \quad \pi_2 = 6 \times 10^8 \text{ water}. \tag{87.2}$$

The length of the domain is 1 m and initially the interface is located at $x = 0.5$ m. The water with density $\rho_2 = 1000$ kg m^{-3} is located on the left side and the air with $\rho_1 = 50$ kg m^{-3} is on the right side. Both fluids have same pressure $p = 10^5$ Pa and velocity $u = 1000$ m s^{-1} at time 0. A small amount of water (respectively gas) $\alpha_2 = 10^{-8}$ is initially present in the gas (respectively water) side. The discretization is done on 1000 cells grid and the CFL number is equal to 0.6. The results are shown at 229 μs. In order to compare the results with those given by another similar diffuse interface method, Fig. 2 displays the mixture density, the pressure, the velocity and the volume fraction for the present reduced model and also for the "five equation-transport model" of [2,12]. For this last model, the numerical method used is the one described in [12]. On this simple test case, the two models are perfectly in agreement and display the same capability to preserve constant velocity and pressure profiles.

5.1.2. Water–air shock tube

We consider a shock tube $[-2,2]$ of 4 m length filled on the left side ($x < 0.7$) with a high pressure liquid water and on the right side with air. This test problem consists of a classical shock tube with two fluids and admits an exact solution. The state laws are the same than in the previous test case. The initial condition consists in a pressure discontinuity between $p = 10^9$ Pa in the liquid side and $p = 10^5$ Pa in the gas side. As in the previous test case, the right and left chambers contain nearly pure fluids: the volume fraction of the gas in the water chamber is $\alpha_1 = 10^{-8}$ and inversely the water volume fraction is $\alpha_2 = 10^{-8}$ in the gas chamber. Again, we compare the results of the present five equation reduced model with those obtained with the "five equation transport model" of [2,12]. Fig. 3 displays for the two models the mixture density, the pressure and the velocity. The exact solutions are represented on these curves by a dotted line. This computation uses a mesh with 1000 cells, with a CFL number equal to 0.6 and the results are shown at time 900 μs. The results for the two models seem to be of comparable accuracy with respect to the exact solution. However, one can notice that the contact discontinuity seems to be more diffused in the "five equation reduced model" while in the "five equation transport model", the shock seems to be slightly in advance with respect to the analytical solution. Fig. 4 that shows an overmagnified region between $x = 1.2$ and $x = 1.3$ shows that this is indeed the case and that the shock speed is not exactly the same for the two models. We emphasize that in the limit of a zero space step, the two models must give identical results. For the present test-case, the contact discontinuity is very close to the shock. Since in the diffusion zone the speeds of sound given by the two models are very different, this can affect the shock speed. For instance at $x = 1.2$, Fig. 4 shows that $\alpha = 0.95$ and thus the sound speed in the "five equation transport model" is equal to 360 m s^{-1} while it is only equal to 260 m s^{-1} in the "five equation reduced model". These results are consistent with Fig. 1 that shows that the speed of sound given by the "five equation transport model" is always larger than the one given by the "five equation reduced model".

Although for this problem, these quantities do not have any physical meaning, it can be of interest to look at the phase quantities ρ_k, ε_k which, respectively, stand for the phase densities and internal energies (cf. Fig. 5). If for the mixture variables the two models have the same behaviour, it is clear that large

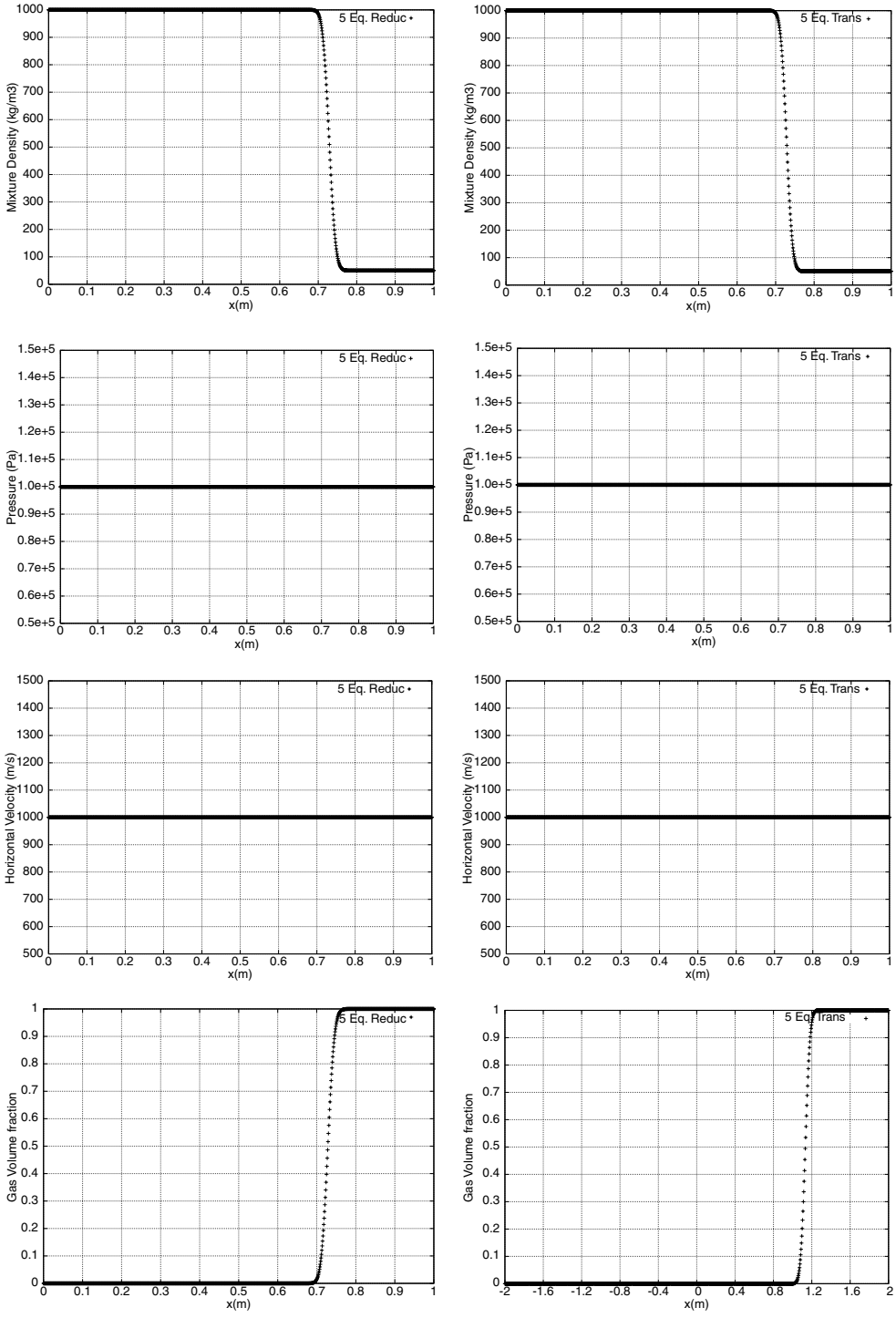

Fig. 2. 5 Equation reduced model (left) and 5 equation transport model (right) in the pure interface advection: mixture variables. Computed solutions with 1000 cells (symbols).

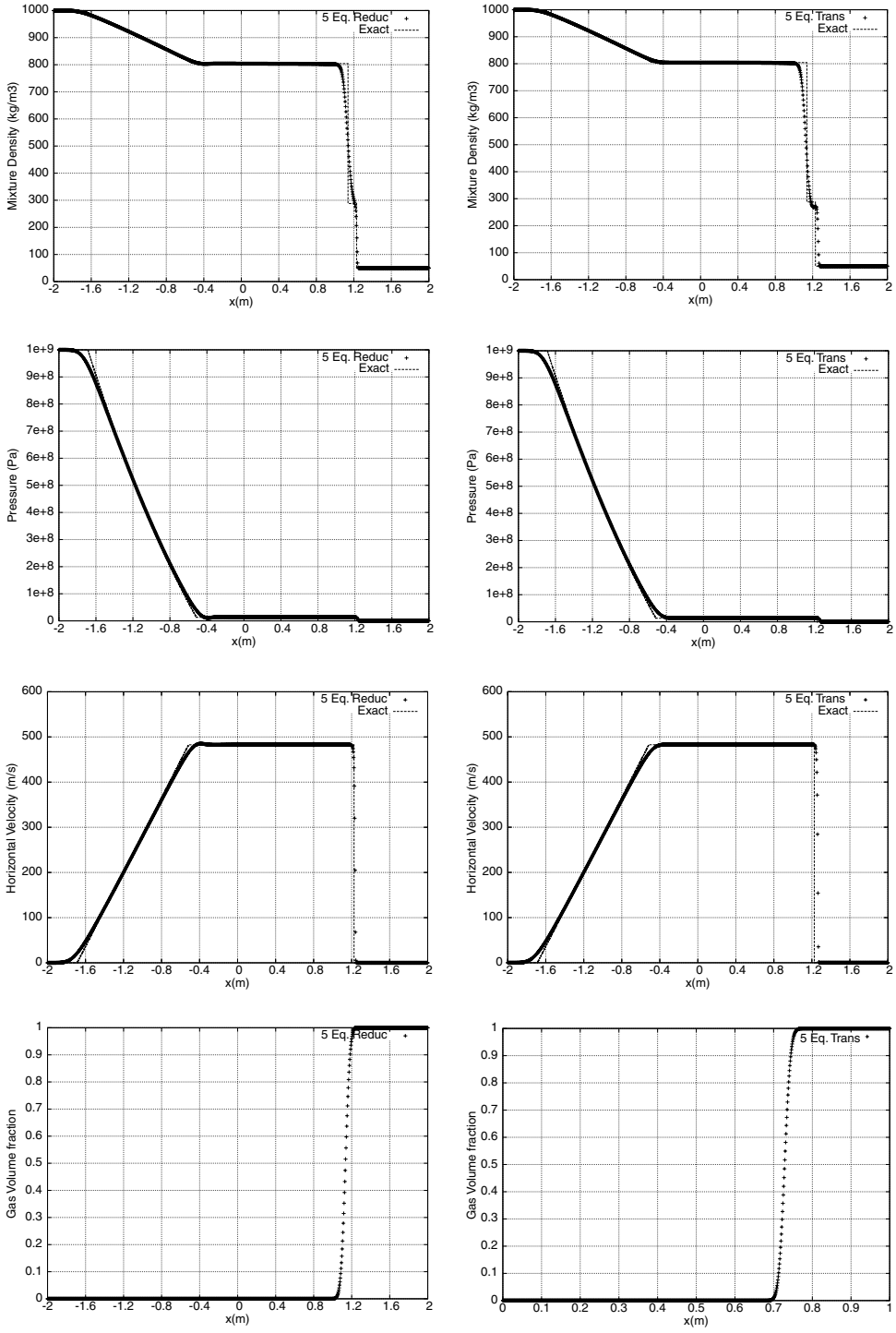

Fig. 3. 5 Equation reduced model (left) and 5 equation transport model (right) in the water–air shock tube: mixture variables. Computed solutions with 1000 cells (symbols) and exact solutions (dotted lines).

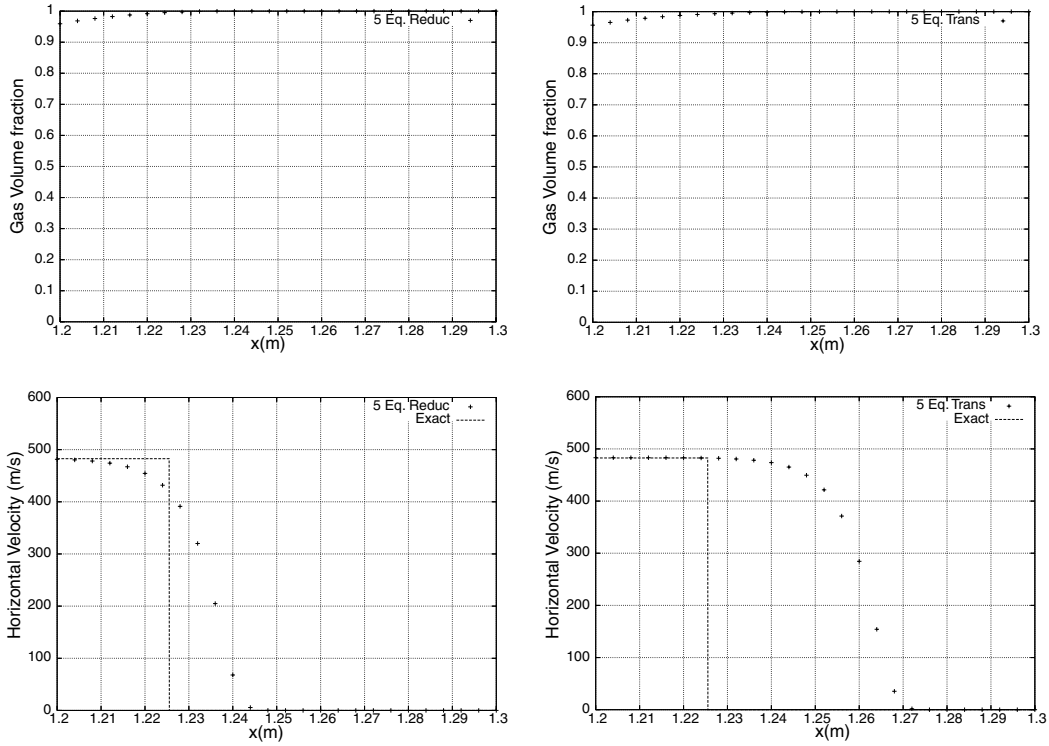

Fig. 4. 5 Equation reduced model (left) and 5 equation transport model (right) in the water–air shock tube: zoom of the shock. Computed solutions with 1000 cells (symbols).

differences can be noticed on the phase quantities between the two models. Finally let us mention that on this test problem, the results on the phase variables are in good agreement with those published for the seven equation model in [16] or in [10]. In particular, the sharp gradient in the air density and internal energy located upstream of the contact discontinuity are also present in the results obtained with the seven equation model. (Compare Fig. 5 (left) with for instance Fig. 7 of [16]).

5.2. Two-phase flow problems: comparison with the seven equation model

5.2.1. First two-phase flow problem

Our second series of numerical experiments deals with two-phase flow and consider problems where the two phases are simultaneously present at the same location. The first experiment considers the same problem than in Section 5.1.2 except that the volume fraction is constant and equal to $\alpha_1 = 0.5$ everywhere in the domain. On the left side ($x < 0.5$) the pressure is 10^9 Pa while it is equal to 10^5 Pa on the right side. The velocity is zero at time 0. Again the discretization is done on a 1000 cells grid and the CFL number is fixed and equal to 0.6. The results are shown at time 200 μs. We compare in Fig. 6 these results with those obtained by the seven equation model of [16]. The numerical method used to solve the seven equation model is the one described in [16], except that the relaxation procedures have been improved as described in [10]. The results are in perfect agreement and this confirms that the present five equation model is a correct asymptotic limit of the seven equation model in the limit of zero relaxation time. In particular, we observe that

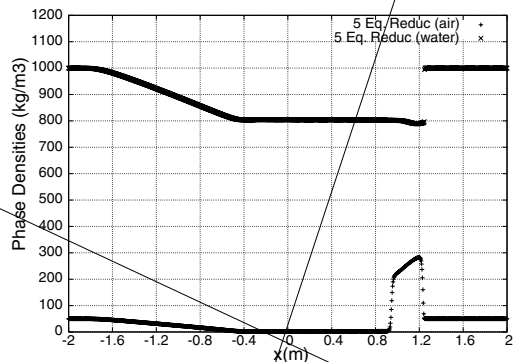

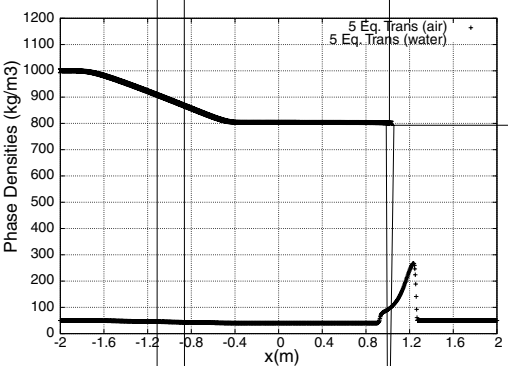

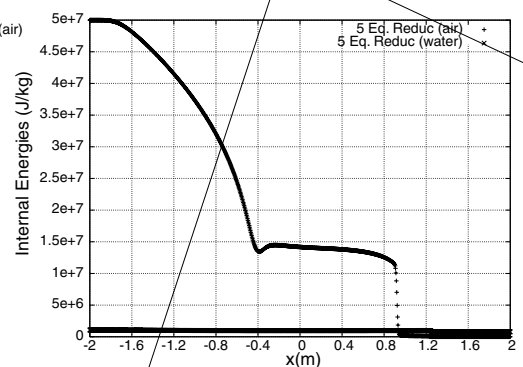

5 Eq. Trans (air)

2.5e+7

1.5e+7

-838 -834 834 162 166

even if the initial composition of the mixture is constant, it evolves in space and time and that this evolution is the same in the results obtained with the two models.

5.2.2. Second two-phase flow problem

The same problem than previously is now considered except that we allow a change in the composition of the mixture. We also change the initial density of the gas for $\rho_1 = 1$ kg m^{-3}. The initial conditions are thus $\rho_1 = 1$ kg m^{-3}, $\rho_2 = 1000$ kg m^{-3}, $u = 0$ m s^{-1} everywhere in the domain while:

$$\begin{cases} p = 10^9 \text{ Pa} & \text{if } x < 0.7, \quad p = 10^5 \text{ Pa} \quad \text{otherwise,} \\ \alpha_1 = 0.2 & \text{if } x < 0.7, \quad \alpha_1 = 0.8 \quad \text{otherwise.} \end{cases}$$

The results are shown at time 200 μs (cf. Fig. 7). The pressure and velocity curves computed with the two models are identical but we notice some differences between the results obtained with the two models in the volume fraction and mixture density profiles. In particular, the post-shock values of the mixture density and volume fraction are not the same and the seven equation model shows an oscillation near the contact discontinuity zone. At the present time, these differences remains unexplainable. Further experiments done by changing the relaxation procedures or the hyperbolic solver in the numerical solution of the seven equation model do not change the results and therefore, it seems that these features are not numerical artifacts but are indeed present in the solution of the seven equation model.

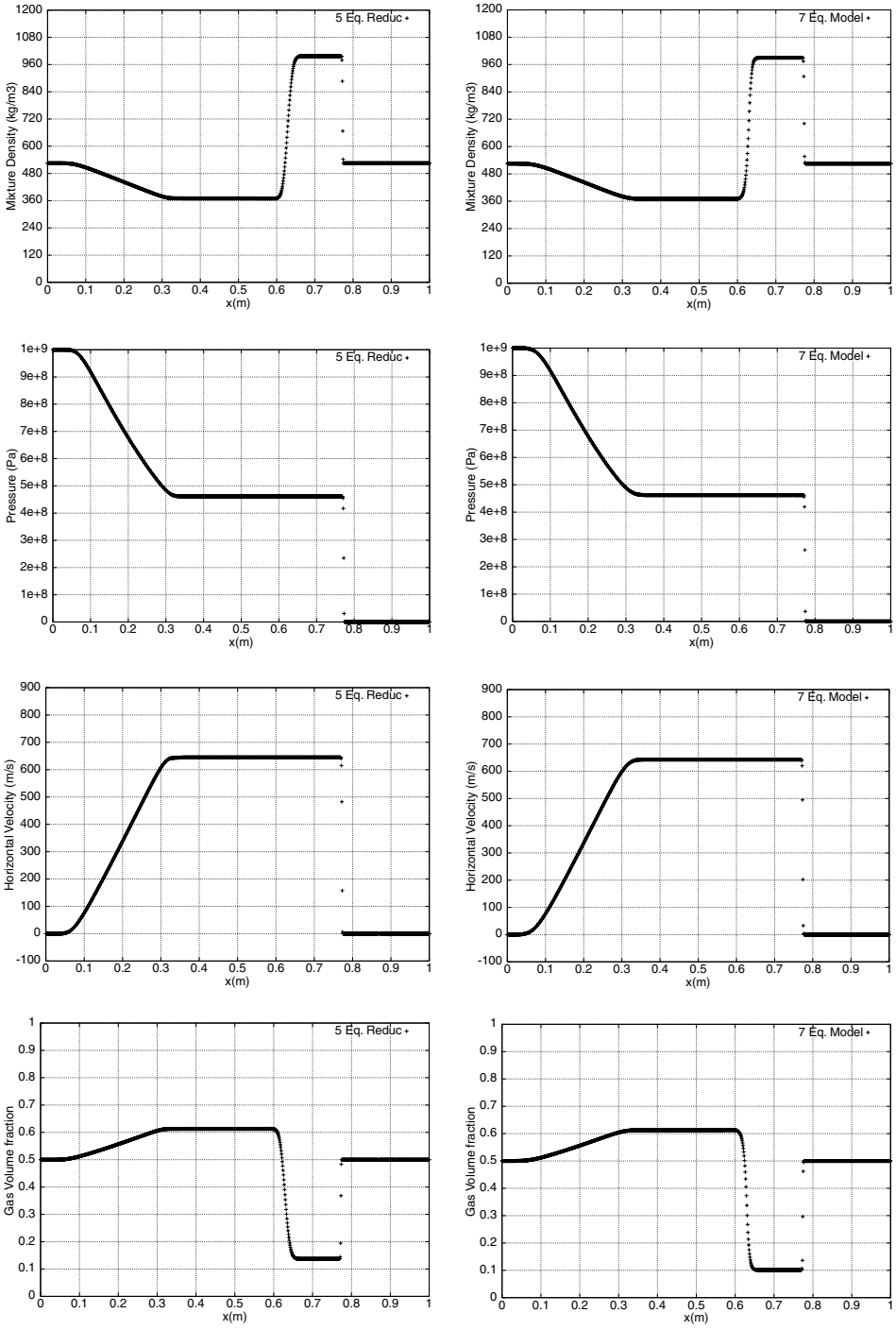

Fig. 6. 5 Equation reduced model (left) and 7 equation model (right) in the first two-phase flow problem. Computed solutions with 1000 cells (symbols).

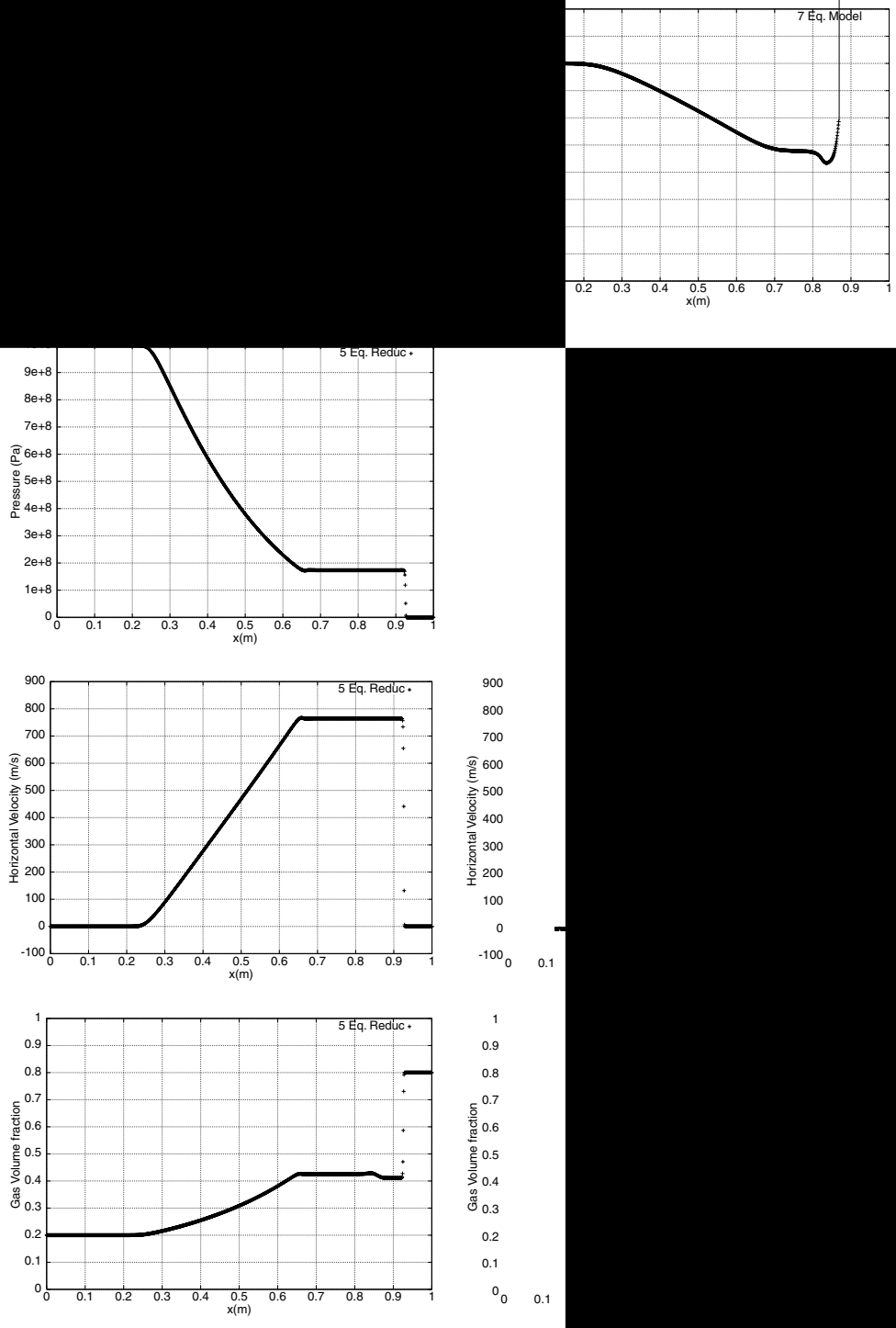

Fig. 7. 5 Equation reduced model (left) and 7 equation model (right) in the secon
1000 cells (symbols).

Fig. 8. Schematic representation of the two-phase impact problem.

5.2.3. Shock propagation in solid alloys

We now evaluate the model capabilities for the computation of shock waves in a two-phase mixture for a test problem involving strong shocks. This type of experiment is particularly important if one want to use the model in DDT studies. Although the model does not admit a full set of Rankine–Hugoniot relations it is possible to solve the equations in an unsteady regime and to determine a numerical velocity of the shock. This will be done in simulating an impact situations in a two-phase mixtures as described in Fig. 8. In order to evaluate the computed results, we will compare them with those obtained with the seven equation model and with experimental data. Actually, for many material, the relation between the shock velocity and the impact velocity is a linear relation, intrinsically characteristic of the material and experimentally determined

$$u_s = a_0 + s u_p, \tag{88}$$

where a_0 is the material sound speed under atmospheric conditions, u_s the shock velocity, u_p the impact velocity and s is a dimensionless constant. The relation (88) is experimentally available for some alloys. Here, we will consider an epoxy/spinel alloy. The equation of state of the two phases are respectively choosen as:

$$p = (\gamma_1 - 1)\rho_1\varepsilon_1 - \gamma_1\pi_1 \quad \text{with } \rho_1 = 1185 \text{ kg m}^{-3}, \quad \gamma_1 = 2.94 \quad \text{and} \quad \pi_1 = 3.2.10^9 \text{ epoxy}, \tag{89.1}$$

$$p = (\gamma_2 - 1)\rho_2\varepsilon_2 - \gamma_2\pi_2 \quad \text{with } \rho_2 = 3622 \text{ kg m}^{-3}, \quad \gamma_2 = 1.62 \quad \text{and} \quad \pi_2 = 141.10^9 \text{ spinel}. \tag{89.2}$$

By computing several unsteady problems with variable impact velocity, we will be able to numerically determine the curve (88) and to compare it with the experimental data. Fig. 9 displays the results at different time = 30, 60 and 90 μs in a computation where the impact velocity is $u_p = 3000$ m s^{-1} and the proportion of epoxy is $\alpha_1 = 0.595$. Several computations of this type give the results shown in Fig. 10. All the computations use a 1000 cells grid and the CFL number is equal to 0.6. We notice a good agreement with the experimental data. We also show in Fig. 10 the results obtained with the seven equation model. We note that the present results are of comparable accuracy with those obtained by this model. Finally, although the five equation model of [2,12] is certainly not suitable for these computations, we have plotted in Fig. 10 the results given by this model. On this test-case, it can clearly be seen that the additional small term present in Eq. (30.5) with respect to the "five equation transport model" has a tremendous influence. Again, we note that these results are consistent with the expressions (29) and (43) of the speed of sound. As discussed in the introduction and in Section 5.1.2, in the case of under-resolved computations, these differences in the value of the speed of sound can appear even in interface simulations.

5.3. Two dimensional tests

We end these series of numerical experiments by some relevant two-dimensional test-cases. These last experiments are computed with a second order MUSCL technique for the space discretization. The time scheme uses the second order, three stage TVD Runge–Kutta discretization described in [18].

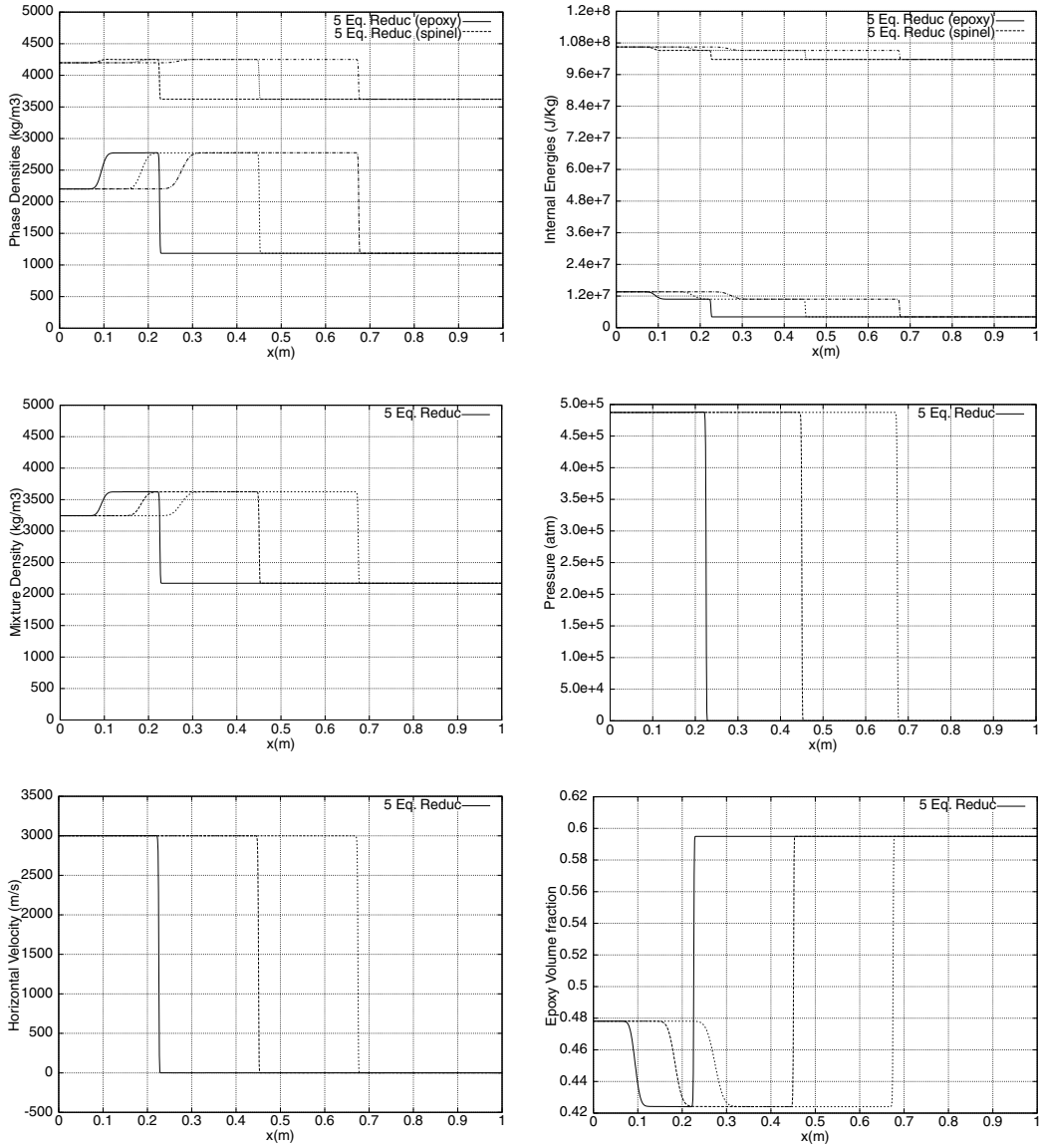

Fig. 9. Results of the 5 equation reduced model for the epoxy/spinel under shock impact at 3000 m/s. Computed solution with 1000 cells.

5.3.1. First two dimensional test: Bubble ascension

This first test shows the ascension of a light air-bubble under the effect of the gravity in a closed box filled with water as described in Fig. 11. Initially the bubble is at rest and the pressure field has an hydrostatic profile. Although it seems simple, this computation presents several numerical difficulties. In particular, the Mach number in this computation is extremely low (it is equal to zero at time $t = 0$ and increases slightly up to a value of 10^{-1} in the course of the computation) and the density ratio between the two fluids is equal to 1000. This is for this test-case that we had to build the acoustic Riemann solver described in Section 4.3.

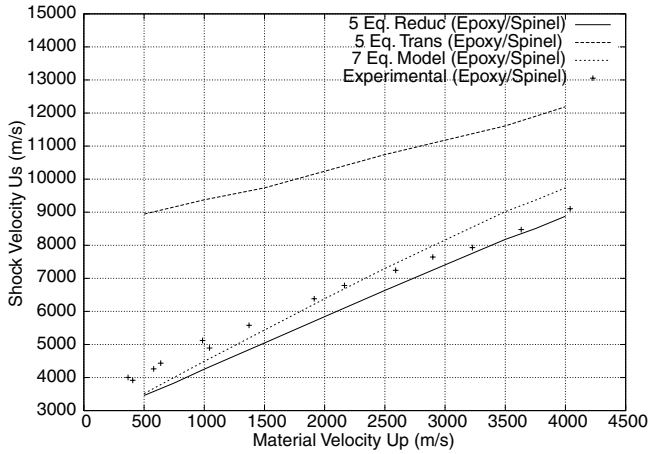

Fig. 10. 5 Equation reduced model (solid line) and 5 equation transport model (dotted line) and 7 equation model (dotted line) in the Mixture Hugoniot (epoxy/spinel) problem and experimental data (symbols).

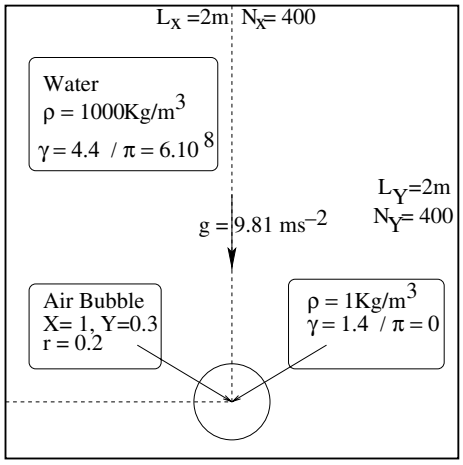

Fig. 11. Initial configuration for the first two dimensional test: Bubble ascension.

The box is 2 m large and 2 m high and the mesh is composed of 400×400 points. Fig. 12 shows the iso-values of the air volume fraction at time = 0, 0.15, 0.35, 0.55, 0.75, 1.0 s. Although this computation would require the introduction of a model of the capillarity forces, the results are very promising. In particular, the numerical diffusion does not prevent the developmental of interface instabilities, the volume fraction remains bounded and the results are perfectly symmetrical with respect to the $x = 1$ axis.

5.3.2. Second two dimensional test

The second test-case is an idealized representation of the sudden heating of a sphere of light material enclosed in a shell of dense one. In opposition with the previous computation, the Mach number in this test-case is large and reaches 0.8. This test case has been initially considered in [12] and will serve to assess the robustness of the numerical method for the computation of large Mach number bi-dimensional flows. In Fig. 13, we present the initial conditions of the problem. The mesh contains 400×400 nodes and the

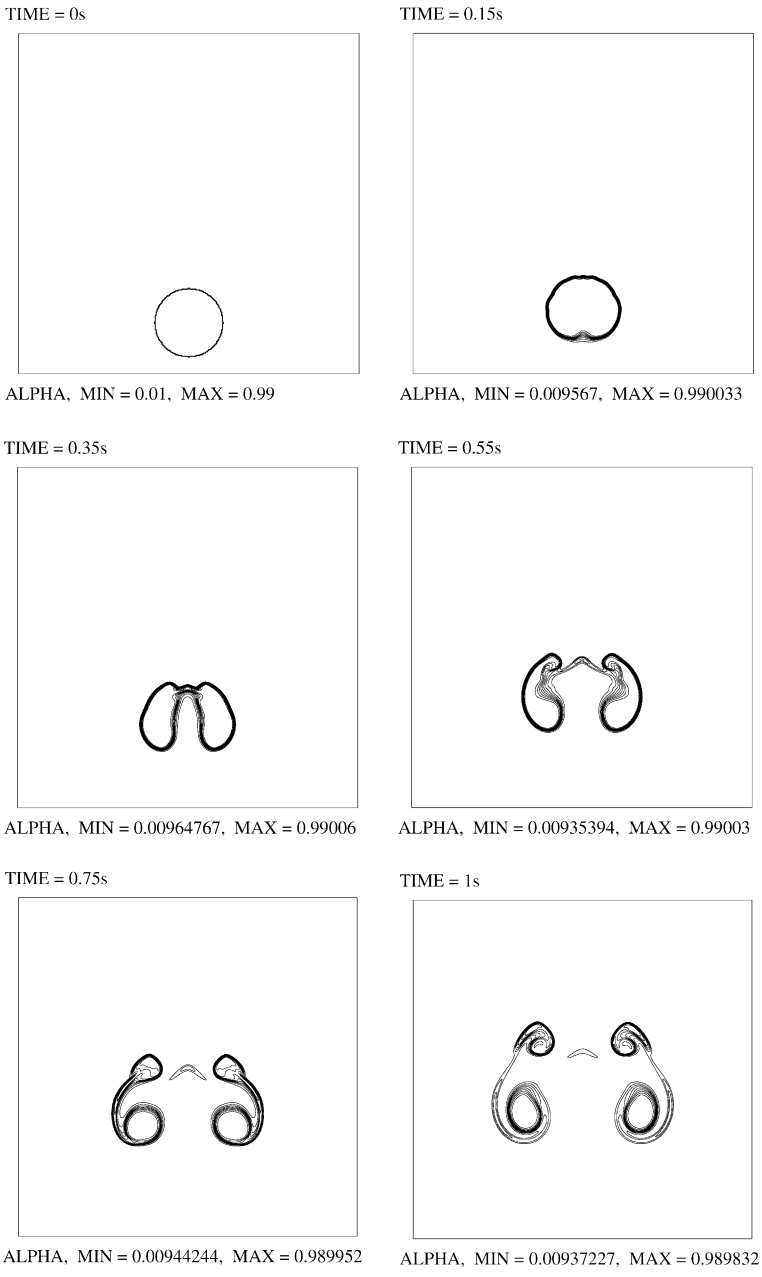

Fig. 12. Isovalues of the volume fraction for the first two dimensional test: Bubble ascension.

CFL number is equal to 0.8. The mesh is regular. Due to the discretization of the circular interfaces, in addition to the development of shock waves in the direction normal to the interfaces, hydrodynamical instabilities of Richtmyer–Meshkov will develop. Fig. 14 shows the isovalues of the volume fraction at time = 0, 1.58, 2.63 ms. We clearly observe the development of these instabilities, producing an intense mixing of the heavy and light fluid near the interface. We also note that although the present results are not

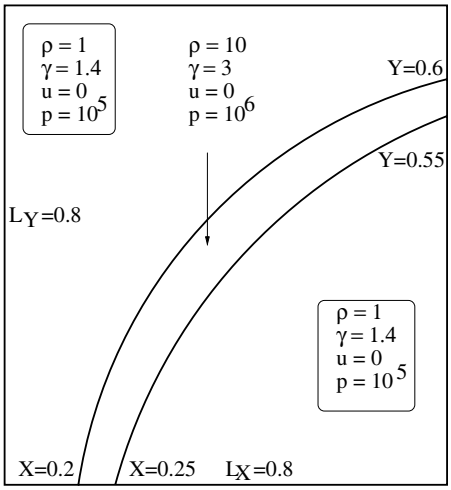

Fig. 13. Initial configuration for the second two dimensional test.

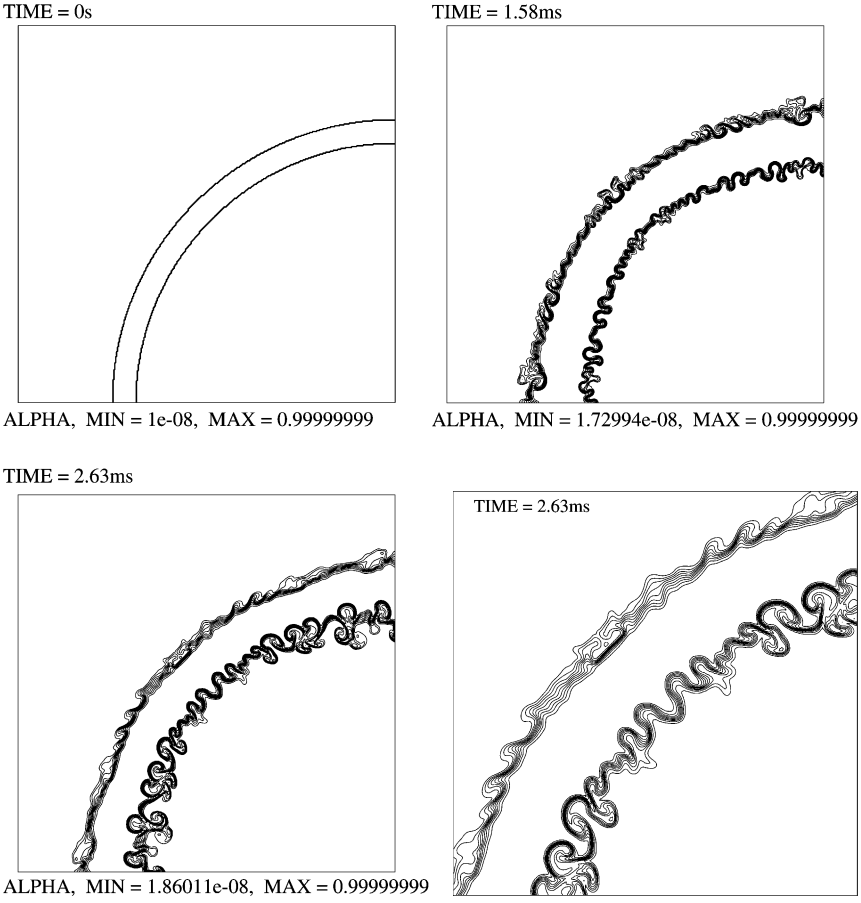

Fig. 14. Isovalues of the volume fraction of the heavy fluid for the second two dimensional test. The right-down plot represents a zoom of the central region at time $t = 2.63$ ms.

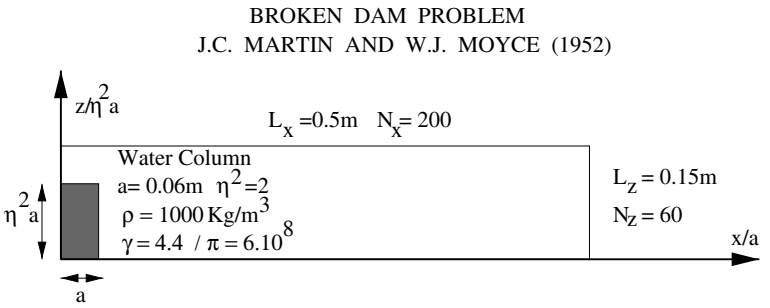

Fig. 15. Initial configuration for the broken dam problem.

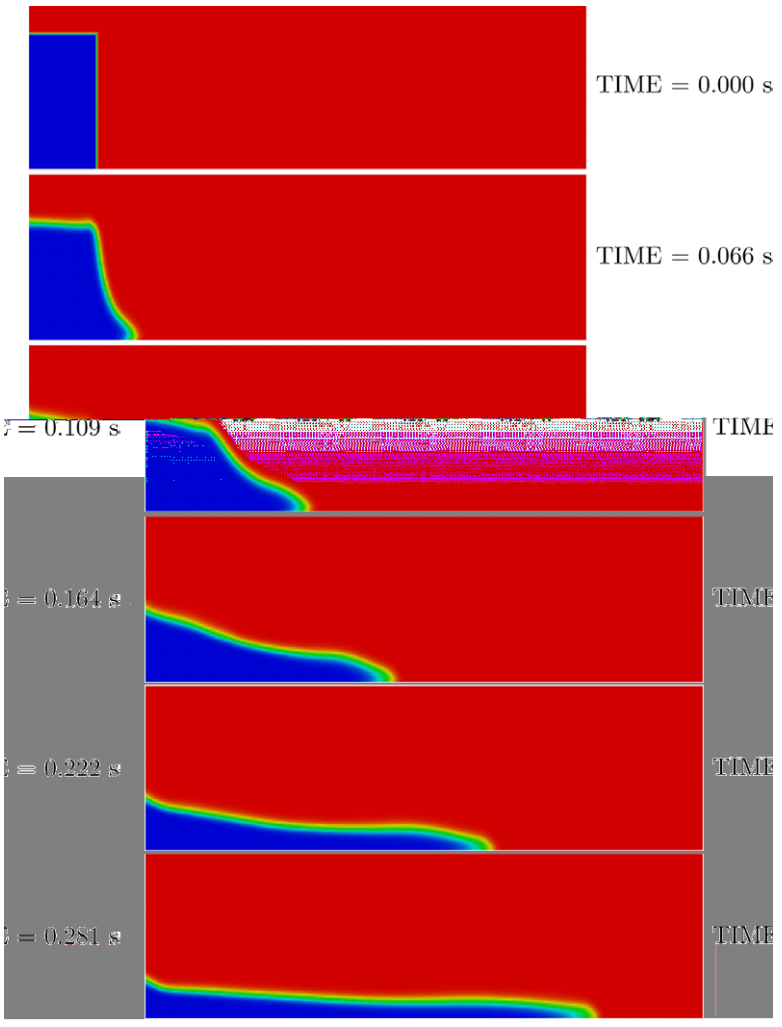

Fig. 16. Isovalues of the volume fraction for the broken dam problem.

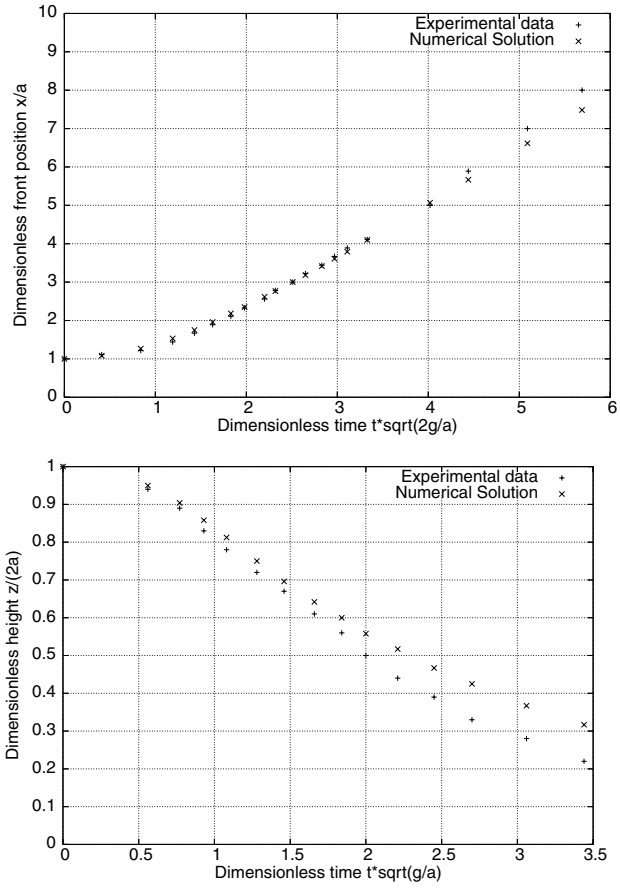

Fig. 17. Comparison between numerical solution and experimental results for the broken dam problem. Front position (top) and height of the column (bottom).

totally identical with those obtained in [12], a good agreement with these results is reached. Again, we emphasize that in the limit where the space step goes to zero, for this interface problems between compressible fluids, the two models have to give exactly the same results. For this computation, a mesh of 400×400 thus seems sufficient for this purpose.

5.3.3. The broken dam problem

Finally, we present here a computation of the well known broken dam problem of Martin and Moyce [11]. This test consists of the simple configuration represented in Fig. 15. Initially a water column with $a = 0.06$ m wide and $\eta^2 a = 0.12$ m high is a rest. All the boundaries are solid walls. Under the effect of the gravity $g = 9.81\ \mathrm{m\,s^{-2}}$, the column collapses. The computation is made with the acoustic solver. The mesh contains 200×60 nodes and the CFL number is equal to 0.8. The experimental results of [11], for the front position $x/a = F_1(\eta^2, t\sqrt{2g/a})$ and the height of the column $z/(\eta^2 a) = F_2(\eta^2, t\sqrt{g/a})$ are used for comparison (note that in the experimental results, the non-dimensional times are different for the front position and the water height: we have used the same non-dimensional units in the presentation of the numerical results to allow a direct comparison with the original publication of [11]). In Fig. 17, are compared the numerical results and the experimental ones for the case $\eta^2 = 2$. Although, the Mach number is

very small, we note a good agreement with the experimental results. Fig. 16 shows the isovalues of the volume fraction at the different dimensionless time $t\sqrt{2g/a} = 0, 1.19, 1.98, 2.97, 4.02, 5.09$ corresponding to the physical times $t = 0$, 0.066, 0.109, 0.164, 0.222, 0.281 s.

6. Conclusion

We have derived a five equation reduced model from an asymptotic analysis in the limit of zero relaxation time of a seven equation two velocity, two pressure model. Although, this model cannot be cast in conservative form, the mathematical structure of the model have been analyzed and shown to be very close to the structure of the Euler equations of fluid dynamics. This model presents an interesting alternative to the use of the seven equation model: it is cheaper, simpler to implement and is easily extensible to an arbitrary number of materials. For instance, in three dimensions, for a number k of different material, the two velocity, two pressure model uses $6k - 1$ variables while the reduced model will use only $2k + 3$ variables.

From a numerical point of view, we have proposed two different approximation schemes of this system. The first one (VFRoe-ncv) relies on an approximate linearized Riemann solver. The second one, that is useful for the simulation of interface problems in low Mach number flows, uses the mathematical structure of the model and relies on the linearization of characteristic relations.

The numerical results show that the reduced five equation model is able of accurate computations of interface problems between compressible material as well as of some two-phase flow problems where pressure and velocity equilibrium between the phases is reached. The numerical methods have been shown to be efficient and robust for a large range of Mach number from almost zero to 1.9 and for density ratio as large as 1000. In the future, we plan to improve the efficiency and accuracy of the numerical method for low Mach number flows by designing implicit and preconditioned schemes for this model. Preliminary results in this direction are promising [13].

Acknowledgements

The work of Angelo Murrone has been supported by a grant of the "Conseil Regional" of region PACA and the CEA Cadarache. Angelo Murrone acknowledges the support of M. Grandotto (CEA Cadarache), P. Gubernatis (CEA Cadarache) and R. Saurel (IUSTI Marseille). He would also like to thank his family for their constant support. We also address a warm thank to M.H. Lallemand for her help with the relaxation procedures in the numerical solution of the seven equation model.

References

[1] R. Abgrall, How to prevent pressure oscillations in multicomponent flow calculations. A quasi conservative approach, J. Comput. Phys. 125 (1996) 150–160.
[2] G. Allaire, S. Clerc, S. Kokh, A five-equation model for the simulation of interfaces between compressible fluids, J. Comput. Phys. 181 (2002) 577–616.
[3] M.R. Baer, J.W. Nunziato, A two-phase mixture theory for the deflagration-to-detonation transition (DDT) in reactive granular materials, J. Multiphase Flow 12 (1986) 861–889.
[4] T. Buffard, T. Gallouët, J.M. Hérard, A sequel to a rough godunov scheme: application to real gases, Comp. Fluid 29 (2000) 673–709.
[5] F. Coquel, J.M. Hérard, N. Seguin, Closure laws for a two-fluid two-pressure model, CR Acad. Sci. Paris, Ser. I 334 (2002) 1–6.
[6] D.A. Drew, S.L. Passman, Theory of multicomponent fluidsApplied Mathematical Sciences, vol. 135, Springer, New York, 1998.
[7] E. Godlewski, P.A. Raviart, Numerical approximation of hyperbolic systems of conservation lawsApplied Mathematical Sciences, vol. 118, Springer, New York, 1995.

[8] M. Ishii, Thermo-fluid dynamic theory of two-phase flow, Direction des études et recherches d'électricité de France, vol. 22, Eyrolles, Paris, 1975.
[9] A.K. Kapila, R. Menikoff, J.B. Bdzil, S.F. Son, D.S. Stewart, Two-phase modelling of DDT in granular materials: reduced equations, Phys. Fluid 13 (2001) 3002–3024.
[10] M.H. Lallemand, R. Saurel, Pressure Relaxation Procedures for Multiphase Compressible Flows, Technical Report 4038, INRIA, 2000.
[11] J.C. Martin, W.J. Moyce, An experimental study of the collapse of liquid columns on a rigid horizontal plane, Phil. Trans. R. Soc. Lond. Ser. A 244 (1952) 312–324.
[12] J. Massoni, R. Saurel, B. Nkonga, R. Abgrall, Propositions de méthodes et modèles Eulériens pour les problèmes à interfaces entre fluides compressibles en présence de transfert de chaleur, Int. J. Heat Mass Trans. 45 (6) (2001) 1287–1307.
[13] A. Murrone, Modèles bi-fluides à six et sept équations pour les écoulements diphasiques à faible nombre de Mach, Ph.D. Thesis, University of Aix-Marseille I, 2003. Available from: http://tel.ccsd.cnrs.fr.
[14] R. Natalini, Recent mathematical results on hyperbolic relaxation problems. Analysis of Systems of Conservation Laws (Aachen, 1997), Chapman and Hall/CRC, Boca Raton, FL, 1999, pp. 128–198.
[15] V.H. Ransom, D.L. Hicks, Hyperbolic two-pressure models for two phase flow, J. Comput. Phys. 53 (1984) 124–151.
[16] R. Saurel, R. Abgrall, A multiphase Godunov method for compressible multifluid and multiphase flows, J. Comput. Phys. 150 (1999) 425–467.
[17] R. Saurel, R. Abgrall, A simple method for compressible multifluid flows, SIAM J. Sci. Comput. 21 (3) (1999) 1115–1145.
[18] C.W Shu, S. Osher, Efficient implementation of essential non oscillatory shock capturing schemes, J. Comput. Phys. 77 (1988) 439–471.
[19] H.B. Stewart, B. Wendroff, Two-phase flow: models and methods, J. Comput. Phys. 56 (1984) 363–409.
[20] E.F. Toro, Riemann Solvers and Numerical Methods for fluid dynamics, Springer-Verlag, Berlin, 1997.
[21] Shaojie Xu, D.S. Stewart, Deflagration-to-detonation transition in porous energetic materials: a comparative model study, J. Eng. Math. 31 (1997) 143–172.